The Report Committee for Sofiane Haythem Achour
Certifies that this is the approved version of the following Report:

Phase Stability Analysis for Tight Porous Media With The Helmholtz Free Energy

APPROVED BY
SUPERVISING COMMITTEE:

Ryosuke Okuno, Supervisor

Kamy Sepehrnoori

Phase Stability Analysis for Tight Porous Media With The Helmholtz Free Energy

by

Sofiane Haythem Achour

Report

Presented to the Faculty of the Graduate School of

The University of Texas at Austin

in Partial Fulfillment

of the Requirements

for the Degree of

Master of Science in Engineering

The University of Texas at Austin

December 2019

Acknowledgements

I am grateful to my supervisor Dr. Ryosuke Okuno for his continuous support and patience. Dr. Okuno's challenging research questions and insights motivated me to work hard and create innovative solutions. I am grateful to Dr. Kamy Spehrnoori for reviewing this report. I would also like to thank Mr. Sajjad S. Neshat and Dr. Gary A. Pope for technical discussions which helped me think about problems from different points of view.

I would also like to gratefully acknowledge the Gas EOR Industrial Affiliates Project at The University of Texas at Austin and the donors of the Thrust 2000 – Flo Wells McGee Endowed Graduate Fellowship in Engineering for their financial support.

Finally, I would like to express my gratitude towards my parents for their guidance. I would like to thank my girlfriend Wendi Liu for her continuous love and support. Lastly, I would like to thank my officemates and friends Jose Mejia, Ricardo Lara, Kwang Hoon Baek, Mingyuan Wang, Javier Santos, and Honggeun Jo for their encouragements, teachings and friendships.

Abstract

Phase Stability Analysis for Tight Porous Media With the Helmholtz Free Energy

Sofiane Haythem Achour, M.S.E

The University of Texas at Austin, 2019

Supervisor: Ryosuke Okuno

Phase stability analysis is commonly used to determine whether a mixture splits into two or more phases at equilibrium. Compositional reservoir simulators use it to initiate phase equilibrium calculations which are necessary to evaluate the amount of oil and gas present in a reservoir. However, conventional methods for stability analysis are not robust when applied to modeling phase behavior in tight reservoirs where equilibrium phase pressures can be different.

Capillary forces in tight reservoirs are strong enough to alter the equilibrium phase compositions and pressures. Phase stability analysis in tight porous media is challenging because it involves predicting the appearance of an additional phase, the pressure of which is initially unknown. This causes common failures of conventional stability analysis

algorithms based on the Gibbs free energy. Due to the lack of robust algorithms, the effects of capillary forces on phase behavior have not yet been included in any commercial software. This is a substantial problem that makes it difficult to accurately model and optimize the production of hydrocarbons from tight reservoirs.

This report presents a new method of phase stability prediction for multicomponent mixtures in tight formation based on the minimization of the Helmholtz free energy. Case studies demonstrate why conventional methods based on the Gibbs free energy are not robust in the presence of capillary pressure. The new method can correctly identify the pressure-temperature region for a given mixture, outside of which the mixture is stable for any capillary pressure.

Table of Contents

List of Tables

List of Figures

CHAPTER 1: Introduction

This chapter describes the type of phase behavior problems solved in this report. Then, it lists the objectives of this research. Lastly, it briefly describes the outline of this report.

1.1 PROBLEM DESCRIPTION

Since 2010, the domestic oil and gas industry has been undergoing a technological revolution associated with the advent of directional drilling and multi-stage hydraulic fracturing. These new technologies allowed operators to produce oil and gas cost-effectively from relatively low permeability reservoirs characterized as "tight". Hydrocarbons produced from those resources contribute about 50% of the domestic crude oil production in 2018. Yet, most of the oil in those reservoirs is being left behind. The ultimate oil recovery at the end of the primary recovery in a tight oil reservoir is only about 5% of the initial reservoir oil volume. Additionally, about 80% of the cumulative oil production is recovered within the first two years. This represents a significant incentive for developing technologies to improve the oil recovery. Miscible solvent injection is one of the most promising methods to achieve that objective where low-cost injection gases are available.

Equation of state (EOS) compositional reservoir simulation is the most reliable way to model oil recovery for miscible solvent injection. A common reservoir simulation technique consists in discretizing a reservoir model containing relevant geological and petrophysical features, and then solving the mass balance equations to compute the flow of fluids between connected reservoir grid blocks in discretized time steps. At every time step, stability analyses estimate the number of equilibrium phases, and phase-split calculations compute the multi-phase equilibrium properties.

It is important for the stability analysis to be robust because it can affect both the computational time and the reliability of the hydrocarbon production prediction. When a phase-stability analysis fails, the mixture is often treated as a stable single phase. Mislabeling unstable phases as stable can cause phase properties to be discontinuous in time and space. This causes errors in the mass-balance equations which can propagate and affect the rest of the simulation. These algorithms can fail by being unable to converge within a given maximum allowable number of iterations. As these calculations are repeated up to millions of times and more, such failures can accumulate and cause significant delays in the computation.

Tight reservoirs are characterized by extremely small pore sizes which magnify the effects of interfacial forces on phase behavior. Pores sizes in tight reservoirs are on the scale of nanometers. At this scale, the curved interfaces that separate equilibrium phases can actually exert pressure on the phase that is on the concave side of the interface. At equilibrium, the difference between the phase pressures due to capillary forces is called the capillary pressure. In tight reservoirs, the higher capillary pressure has a strong effect on the phase behavior of oil and gas mixtures. However, commercial reservoir simulators do not even attempt to include this effect because there is no robust method of implementing it. As will be explained in this report, there are some inconsistency and inaccuracy regarding the formulation of phase stability under capillary pressure in the literature.

The effect of capillary forces on oil recovery from miscible solvent injection is little understood partly because of the lack of robust numerical equilibrium calculation methods including the effects of capillary pressure. The existing theory is mostly based on advection-dominated flow with negligible capillary pressures. However, both fundamental assumptions are questionable in tight porous media. The development of robust stability

analysis for tight porous media is therefore an important and necessary step toward understanding solvent injection enhanced oil recovery.

1.2 Research Objectives

The robustness of stability analysis algorithms strongly depends on the formulation. Most algorithms used for tight reservoirs analyze the Gibbs free energy of hypothetical phases in order to predict the stability of a given mixture. One important variable which defines this Gibbs free energy is the pressure of the incipient phase. Therefore, numerical methods must estimate the capillary pressure iteratively during the stability test in order to determine the pressure of the incipient phase. These iterative estimations make the stability analysis algorithm less reliable and often fail for practical applications.

Reservoir simulators which do not include the effect of capillary pressure manage to reduce their computational time by only running stability tests for mixtures that are near the limit of instability. Since the capillary pressure is initially unknown and defines the Gibbs free energy of the incipient phase, this operation can only be done by initially assuming a null capillary pressure. This assumption can sometimes lead to erroneous result of the stability test.

The main objective of this research is to develop a robust stability test for tight reservoirs. This is done by removing the dependency of the free energy function on pressure. We accomplish that by using the Helmholtz free energy instead of the Gibbs free energy. We then demonstrate the advantages of using this thermodynamic function through some concrete examples. Finally, we demonstrate that using the Helmholtz free energy is not only reliable, but also potentially useful for speeding up the compositional reservoir simulation.

1.3 OUTLINE OF REPORT

This report consists of four chapters. Chapter 2 derives the basics of phase equilibrium calculations from the first and second laws of thermodynamics. The formulation for stability analysis using the Gibbs and the Helmholtz free energies are presented. Basics of minimization algorithms and cubic equations of state are then described. After that, a literature review is given on phase stability analysis for tight reservoirs using both free energy functions.

In Chapter 3, we develop a new algorithm for phase-stability analysis that can be used with any capillary pressure model. The robustness of our algorithm is explained and demonstrated by comparing it with the conventional algorithm in come case-studies.

Chapter 4 summarizes and concludes the research. Recommendations for future research are also presented.

CHAPTER 2: Background

This chapter explains the required basics for phase equilibrium calculations in tight porous media and gives a literature review. The first part of this chapter derives fundamental thermodynamic conditions characterizing phase equilibrium in tight reservoirs and the correlations used for their computations. The second part reviews the various challenges and solutions that have been proposed to solve the phase equilibrium problems in tight reservoirs.

2.1 Basics of Capillary Equilibrium Calculations

This section explains the required basics for phase stability analysis for tight reservoirs. The first part of this chapter derives fundamental equations to be satisfied at phase equilibrium. The second part discusses the conventional formulations and algorithms for stability analysis. Next, it introduces equations of state and capillary pressure models that are used to compute the state of a mixture for given conditions. Finally, it introduces general numerical methods that are used in stability analysis algorithms.

2.1.1 Phase Equilibrium Conditions

This section lays out the fundamentals required for understanding thermodynamic equilibrium. Although some of the definitions and equations presented in this section may not be consistent with those most commonly used in the literature, they are consistent with those used by Gibbs (1878) who first introduced these concepts.

The first law of thermodynamics states the total energy of an isolated system is constant. For non-isolated systems, energy can be transferred in the form of heat, work, or mass flow

$$d\mathrm{U} = d\mathrm{Q} + d\mathrm{W} + d\mathrm{E}, \tag{2.1}$$

where U is the internal energy, Q is heat, W is work, E is the potential energy contribution carried by the flow of matter into the system, and d corresponds to an infinitesimal positive change.

According to the second law of thermodynamics, the state of an isolated system spontaneously changes only to maximize its total entropy. For a heterogeneous isolated system composed of a homogeneous subsystem and its surroundings, the total entropy change is

$$dS_{\mathrm{total}} = dS + dS' \geq 0 \text{ for } dU_{\mathrm{total}} = 0, \tag{2.2}$$

where U_{total}, S, and S' are the total internal energy of the isolated system and the entropies of the subsystem and its surroundings within the isolated system respectively.

A necessary and sufficient condition for an isolated system at equilibrium is that any alteration that does not change its total energy can only result in a negative or null change of its entropy, therefore $d^2S < 0$ at equilibrium. The entropy change of the surroundings is related to the heat flow $dS' = dQ'/T' = -dQ/T$. This leads to the Clausius inequality,

$$dS \geq dQ/T. \tag{2.3}$$

A process is called reversible when it does not lead to an increase in the total entropy of a thermodynamic system. It follows that all infinitesimally small changes about the equilibrium state of a system are reversible. According to equations (2.2) and (2.3), the entropy change of a system caused by a reversible process is related to the heat flow from its surroundings is then $dS = dQ/T$.

Equations (2.1) and (2.3) can be used to derive the conditions for spontaneous change with the internal energy of a system

$$dU \leq TdS + YdX + \sum_{i=1}^{N_c} \mu_i dn_i, \tag{2.4}$$

where $Y dX$ represents the work dW done on the system exerted by general distributed force Y to deform the system by a generalized displacement dX. $\mu_i dn_i$ represents the chemical energy flow dE originating from an increase dn_i in the amount of substance i carrying the chemical potential energy μ_i such that $i = 1,2,3, \dots, N_c$ and the total number of substances (or components) in the system is denoted as N_c. The amount of substance i can be quantified by its number of moles. For reversible processes, the inequality relation (2.4) becomes equality.

In this research, we consider two types of work which can be done on the system. The first one happens when a pressure P is applied on the boundaries of the system to reduce its volume by $-dV$. Work can also be done on a system by applying an interfacial tension σ on the boundaries of a system to increase the surface area by da. Bulk phases are three-dimensional systems which cannot be subject to interfacial work. Similarly, interfaces are two-dimensional systems which separate two equilibrium phases and cannot be subjected to volumetric work. When studying equilibrium in small media, the interfacial volume may not be negligible and can therefore be subjected to volumetric work. In those cases, the term "interphase" is used instead of "interface".

Some Maxwell relations can be derived from inequation (2.4) for reversible processes by using the chain-rule for the total differential of the internal energy U.

$$\left(\frac{\partial U}{\partial S}\right)_{X,\underline{\mathbf{n}}} = T, \qquad \left(\frac{\partial U}{\partial X}\right)_{S,\underline{\mathbf{n}}} = Y, \qquad \left(\frac{\partial U}{\partial n_i}\right)_{S,X,n_{j\neq i}} = \mu_i \tag{2.5}$$

The subscripts of the partial derivatives in equation (2.5) indicate the variables held constant while evaluating the partial derivative. The symbol $\underline{\mathbf{n}}$ is used to represent a vector containing the values for number of moles of each component in a mixture. The subscript $n_{j\neq i}$ is used as a short-hand notation here to indicate that the total number of moles of all components $j = 1,2, \dots, i-1, i+1, \dots, N_c$ are being held constant in the evaluation of the partial derivative.

The internal energy is an extensive, additive property of a system dependent on the extensive additive properties S, V, and $\underline{\mathbf{n}}$. It follows that for any real scalar quantity λ,

$$\mathrm{U}\left(\lambda \mathrm{S}, \lambda \mathrm{V}, \lambda \underline{\mathbf{n}}\right) = \lambda \mathrm{U}\left(\mathrm{S}, \mathrm{V}, \underline{\mathbf{n}}\right),$$

where the intensive thermodynamic variables are the same for the state on the right and left-hand side of the equation above. By integrating the derivative of equation (2.4) with respect to λ for an equilibrium system supposing that the λ varies from 0 to 1, we obtain

$$\mathrm{U} = \mathrm{TS} + \mathrm{YX} + \sum_{\mathrm{i}=1}^{\mathrm{N_c}} \mu_{\mathrm{i}} \mathrm{n}_{\mathrm{i}}. \tag{2.6}$$

If we subtract a differential element of U in equation (2.6) from dU equation in (2.4) for a reversible process, we obtain the Gibbs-Duhem equation as derived by Gibbs (1878)

$$0 = \mathrm{S}d\mathrm{T} + \mathrm{X}d\mathrm{Y} + \sum_{\mathrm{i}=1}^{\mathrm{N_c}} \mathrm{n}_{\mathrm{i}} d\mu_{\mathrm{i}}. \tag{2.7}$$

The Helmholtz free energy is defined as $\mathrm{A} = \mathrm{U} - \mathrm{TS}$. From equation (2.4), the change of Helmholtz free energy of a system is

$$d\mathrm{A} \leq -\mathrm{S}d\mathrm{T} + \mathrm{Y}d\mathrm{X} + \sum_{\mathrm{i}=1}^{\mathrm{N_c}} \mu_{\mathrm{i}} d\mathrm{n}_{\mathrm{i}}. \tag{2.8}$$

According to the definition of the Helmholtz free energy and the equation (2.6), $\mathrm{A} = \sum_{\mathrm{i}=1}^{\mathrm{N_c}} \mu_{\mathrm{i}} \mathrm{n}_{\mathrm{i}} - \mathrm{PV} + \sigma \mathrm{a}$. The Helmholtz free energy change for a system held at a constant temperature, with no deformation of the system, and constant amount of matter is $d\mathrm{A} \leq 0$. As a result, the necessary and sufficient condition for the equilibrium of this system is that the equilibrium solution is at a global minimum of A. This condition requires that $d^2\mathrm{A} > 0$ and $d\mathrm{A} = 0$ at equilibrium.

We define the Gibbs free energy as $\mathrm{G} = \mathrm{U} - \mathrm{TS} + \mathrm{PV} - \sigma \mathrm{a}$. From equations (2.4) and (2.5), the change of Gibbs free energy of a system is then

$$d\mathrm{G} \leq -\mathrm{S}d\mathrm{T} + \mathrm{V}d\mathrm{P} + \mathrm{a}d\sigma + \sum_{\mathrm{i}=1}^{\mathrm{N_c}} \mu_{\mathrm{i}} d\mathrm{n}_{\mathrm{i}} \tag{2.9}$$

We define partial properties of thermodynamic variables as the derivative of the said property with respect to the number of moles of component i at a fixed temperature and generalized distributed force. Let us denote $\overline{\mathcal{M}_{\mathrm{i}}}$ as the partial property of $\mathcal{M}$ for

component i where $i = 1, \dots, N_c$ defined as $\overline{\mathcal{M}_i} = (\partial \mathcal{M} / \partial n_i)_{T,Y,n_{k \neq i}}$. We then notice from inequation (2.9) for a reversible process that $\overline{G_i} = (\partial G / \partial n_i)_{T,Y,n_{k \neq i}} = \mu_i$.

According to the definition of the Gibbs free energy and the equation (2.6), $G = \sum_{i=1}^{N_c} \overline{G_i} n_i$. The Gibbs free energy of a system held at a constant temperature, pressure, interfacial tension, and amount of matter is $dG \leq 0$. As a result, the necessary and sufficient conditions for the equilibrium of this system is that the equilibrium solution is at a global minimum of G. This condition requires that $d^2G > 0$ and $dG = 0$.

We now derive more specific phase equilibrium conditions for multiphase multicomponent system held at a fixed pressure, interfacial tension, temperature, and amount of substance for each component. The differential reversible change for the total Gibbs free energy of a mixture of N_c components, N_p bulk phases, and N_f interphases and can be written as

$$\begin{aligned} dG = \sum_{j=1}^{N_t} [& \left(\partial G_j / \partial T_j\right)_{P_j,\sigma_j,\underline{n}_j} dT_j + \left(\partial G_j / \partial P_j\right)_{T_j,\sigma_j,\underline{n}_j} dP_j \\ & + \left(\partial G_j / \partial \sigma_j\right)_{T_j,P_j,\underline{n}_j} d\sigma_j + \sum_{i=1}^{N_c} \left(\partial G_j / \partial n_{ij}\right)_{T_j,P_j,\sigma_j,n_{k \neq i,j}} dn_{ij}] \end{aligned} \tag{2.10}$$

where $N_t = N_p + N_f$.

Each derivative in equation (2.10) is a Maxwell relation which can be derived from inequation (2.9) for a reversible process. The reversible change in the Gibbs free energy for a closed system held at a constant uniform temperature T, pressure P, and interfacial tension σ can then be derived as

$$dG = \sum_{j=1}^{N_s} \sum_{i=1}^{N_c} \overline{G_{ij}} dn_{ij}. \tag{2.11}$$

The first-order condition for a stable system at the minimum of the Gibbs free energy is that the gradient of the Gibbs free energy with respect to mole numbers of component i in phase/interphase j is equal to 0. Because the system is closed, the total number of moles of each component in the system is constant. This constraint results in

one less degree of freedom for the number of moles of each component in the arbitrary phase/interphase N_t such that

$$n_{iN_t} = n_i - \sum_{j=1}^{N_t-1} n_{ij} \text{ where } i = 1, \dots N_c.$$

Therefore, we have

$$\partial n_{ij}/\partial n_{ik} = \begin{cases} 1, \text{for } j = k \\ 0, \text{for } j \neq k \text{ and } j \neq N_t \\ -1, \text{for } j = N_t \end{cases} \text{ where } i = 1, \dots, N_c \tag{2.12}$$

Equation (2.12) can then be used to evaluate the derivative of the Gibbs free energy of the system with respect to the number of moles of component i in phase/interphase j.

$$\left(\partial G/\partial n_{ij}\right)_{n_{k\neq i,j}} = \overline{G}_{ij} - \overline{G}_{iN_t}, i = 1, \dots N_c \tag{2.13}$$

The first-order condition for stability of a multiphase mixture at a minimum of the Gibbs free energy is therefore that the chemical potentials of each component i ($i = 1, \dots, N_c$) are equal for all phases/interphases j ($j = 1, \dots, N_t$). This equality is equivalent to the working equation for phase equilibrium calculations

$$f_{ij} = f_{iN_t}, \tag{2.14}$$

where f_{ij} is the fugacity of component i in phase/interphase j. The fugacity is defined as

$$f_{ij} = x_{ij} P_j \exp\left((\overline{G}_{ij} - \overline{G}_{ij}^{IGM})/RT\right), \text{ where } i = 1, \dots, N_c \text{ and } j = 1, \dots, N_t. \tag{2.15}$$

x_{ij} and $\overline{G}_{ij}^{IGM}$ are the mole fractions and partial molar Gibbs free energy of an ideal gas mixture for component i in phase/interphase j respectively, P_j is the pressure of phase j, and R is the ideal gas constant. The ideal gas mixture partial molar Gibbs free energy is equal to that of the real mixture at $P \to 0$. It follows from equation (2.11) that $d\overline{G}_{ij} = -\overline{V}_{ij} dP_j$. Therefore, the fugacity of a phase can be written as

$$\ln(\phi_{ij}) = \ln\left(f_{ij}/(x_{ij}P_j)\right) = (RT)^{-1} \int_0^{P_j} \left(\overline{V}_{ij} - RT/P\right) dP. \tag{2.16}$$

The first-order condition for multiphase multicomponent equilibrium for a system held at a constant temperature, total volume, interfacial areas and total number of moles

can be derived using the Helmholtz free energy. The reversible change of the Helmholtz free energy is

$$dA = \sum_{j=1}^{N_s}[\left(\partial A_j/\partial T_j\right)_{V_j,a_j,\underline{n}_j} dT_j + \left(\partial A_j/\partial a_j\right)_{V_j,T_j,\underline{n}_j} da_j + \left(\partial A_j/\partial V_j\right)_{V_j,T_j,\underline{n}_j} dV_j + \sum_{i=1}^{N_c}\left(\partial A_j/\partial n_{ij}\right)_{V_j,a_j,T_j,n_{k\neq i,j}} dn_{ij}]. \quad (2.17)$$

Each derivative in equation (2.17) is a Maxwell relation which can be derived from inequation (2.8) for a reversible process. The reversible change in Helmholtz free energy for a closed system held at a constant uniform temperature T can then be derived as

$$dA = \sum_{j=1}^{N_s} \sigma_j da_j - P_j dV_j + \sum_{i=1}^{N_c} \overline{G}_{ij} dn_{ij}. \quad (2.18)$$

We distinguish two kinds of interphases. The first is the interphase between two fluid phases at equilibrium. The maximum number of such interphases is equal to $\sum_{j=1}^{N_p-1} j$. The second kind of interphase is that which separates equilibrium phases and the boundaries of the system s. The maximum number of such interphases is equal to N_p. Depending on the definition of the system, different types of surface areas may be held constant to minimize the Helmholtz free energy. The most appropriate system for porous media is one where the total area of the boundaries of the system is held constant while the other constraints determine the total fluid-fluid area at equilibrium. For the following derivation, we assume that the volume of the interphase is negligible.

For a system held at a constant temperature T, total number of moles of each component $\underline{\mathbf{n}}$, total volume V, and interfacial areas a_s with the boundaries of the system, the number of independent variables is decreased such that

$$V_{N_p} = V - \sum_{j=1}^{N_p-1} V_j,$$

$$a_{sN_p} = a_s - \sum_{j=1}^{N_p-1} a_{sj},$$

$$n_{iN_s} = n_i - \sum_{j=1}^{N_s-1} n_{ij} \text{ where } i = 1, \ldots N_c,$$

where a_{sj} is the area of the interphase between the boundary of the system s and phase j. Therefore,

$$\partial n_{ij}/\partial n_{ik} = \begin{cases} 1, \text{for } j = k \\ 0, \text{for } j \neq k \text{ and } j \neq N_s \\ -1, \text{for } j = N_s \end{cases} \tag{2.19}$$

$$\partial n_{ij}/\partial n_{lk} = 0 \text{ for } i \neq l$$

$$\partial V_j/\,\partial V_k = \partial a_{sj}/\,\partial a_{sk} = \begin{cases} 1, \text{for } j = k \\ 0, \text{for } j \neq k \text{ and } j \neq N_p \text{ , } i = 1, \ldots N_c \\ -1, \text{for } j = N_p \end{cases}$$

Equations (2.19) can then be used to evaluate the derivatives of the Helmholtz free energy

$\partial A/\partial n_{ij} = \overline{G}_{ij} - \overline{G}_{iN_t}$, where $i = 1, \ldots N_c$ and $j = 1, \ldots N_t$, and

$$\partial A/\partial V_j = P_{N_p} - P_j + \sigma_{jN_p}\,\partial a_{jN_p}/\,\partial V_j + \left(\sigma_{sj} - \sigma_{sN_p}\right)\partial a_{sj}/\,\partial V_j, \tag{2.20}$$

where $j = 1, \ldots N_p$.

The first-order condition for stability of a multiphase mixture at a minimum of the Helmholtz free energy is that the derivatives are equal to 0, hence

$$\overline{G}_{ij} - \overline{G}_{iN_t} = 0, \text{ where } i = 1, \ldots N_c \text{ and } j = 1, \ldots, N_t - 1, \tag{2.21}$$

$$P_j - P_{N_p} = \sigma_{jN_p}\,\partial a_{jN_p}/\,\partial V_j + \left(\sigma_{sj} - \sigma_{sN_p}\right)\partial a_{sj}/\,\partial V_j \text{ where } j = 1, \ldots, N_p. \tag{2.22}$$

The terms da_{js}/dV_j and $\partial a_{jN_s}/\,\partial V_j$ refer to the change in interfacial area in the porous medium as the volume of phase j increases by displacing phase N_p. Note that the equilibrium condition (2.22) is the same as that for the Gibbs free energy in equation (2.14).

According to equation (2.8), for a system constrained by a fixed volume temperature and number of moles, the area is minimized at equilibrium in order to minimize the total Helmholtz free energy. This is accomplished by contracting into spherical shapes. The interfacial tension causes these curved interfaces to exert a net contractile force on the phase which is on the concave side of the interface. This net distributed force is called the capillary pressure P_{cap}, and is equal to the difference in pressure between two equilibrium phases. At equilibrium, the magnitude of the capillary pressure is defined by equation (2.22). By convention, the sign of the capillary pressure is

defined as the difference in equilibrium pressure between the lowest-density phase and the highest-density phase (Lake, 2014),

$$\mathrm{P_{cap}} = \mathrm{P_1} - \mathrm{P_2}, \text{ such that } \rho_1 < \rho_2 \tag{2.23}$$

where ρ_j is the mass density of phase j.

Equilibrium thermodynamic relations are conservative functions therefore, they must hold true for any set of constraints. For example, the equilibrium state of a system as specified by a fixed pressure, temperature, and composition at the minimum of the Gibbs free energy must be the same as that specified by a fixed temperature, total volume and composition at the minimum of the Helmholtz free energy. Due to this principle, the capillary pressure as derived in equation (2.22) must be the same as a system where the contributions from the walls are neglected so long as the interface area and tension are the same. For a two-phase system where the energy contribution from the boundaries is neglected, the change of Helmholtz free energy becomes

$$d\mathrm{A} = -\mathrm{P_1}d\mathrm{V_1} - \mathrm{P_2}d\mathrm{V_2} + \sigma_{12}d\mathrm{a_{12}} + \sum_{\mathrm{i=1}}^{\mathrm{N_c}} \overline{\mathrm{G}}_{\mathrm{i1}} d\mathrm{n_{i1}} + \sum_{\mathrm{i=1}}^{\mathrm{N_c}} \overline{\mathrm{G}}_{\mathrm{i2}} d\mathrm{n_{i2}}. \tag{2.24}$$

In a system where the total volume and number of moles of each component are held constant, derivatives in terms of volume and mole numbers in equation (2.19) remain valid. The change of the Helmholtz free energy for that constrained system is

$$d\mathrm{A} = (\mathrm{P_2} - \mathrm{P_1} + \sigma_{12}d\mathrm{a_{12}}/d\mathrm{V_1})d\mathrm{V_1} + \sum_{\mathrm{i=1}}^{\mathrm{N_c}} (\overline{\mathrm{G}}_{\mathrm{i1}} - \overline{\mathrm{G}}_{\mathrm{i2}}) d\mathrm{n_{i1}}. \tag{2.25}$$

According to the second law of thermodynamics, the first order condition for equilibrium in this system is the stationarity of the Helmholtz free energy

$$\mathrm{P_1} - \mathrm{P_2} = \sigma_{12}d\mathrm{a_{12}}/d\mathrm{V_1}. \tag{2.26}$$

The term $d\mathrm{a_{12}}/d\mathrm{V_1}$ is equal to the rate of change of the surface area of a bubble as the volume of phase 1 increases. The magnitude of the capillary pressure evaluated using equation (2.22) must the same as that with equation (2.26). Therefore, the terms

$\sigma_{12} d\mathrm{a}_{12}/d\mathrm{V}_1$ from equations (2.22) and (2.26) are not equal. Equation (2.26) can be evaluated for a spherical interface of curvature radius $\mathcal{R}$.

$$\left|\mathrm{P}_{\mathrm{cap}}\right| = \sigma_{12}\left|(d\mathrm{a}_{12}/d\mathcal{R})(d\mathrm{V}_1/d\mathcal{R})\right| = 2\sigma_{12}/\mathcal{R} \tag{2.27}$$

Capillary pressure affects the equilibrium phase properties due to the dependence of the partial molar Gibbs free energy on pressure. The partial molar Gibbs free energy equality in the presence of capillary pressure for a two-phase system is then

$\overline{\mathrm{G}}_{\mathrm{i}1}(\mathrm{P}_1) = \overline{\mathrm{G}}_{\mathrm{i}2}(\mathrm{P}_1) + \int_{\mathrm{P}_1}^{\mathrm{P}_2} \overline{\mathrm{V}}_{\mathrm{i}2} d\mathrm{P}$, where $\mathrm{i} = 1, \ldots \mathrm{N}_{\mathrm{c}}$.

The magnitude of the term $\int_{\mathrm{P}_1}^{\mathrm{P}_2} \overline{\mathrm{V}}_{\mathrm{i}2} d\mathrm{P}$ represents the magnitude of the deviation of the equilibrium states from equilibrium at no capillary pressure. Therefore, for large values of $|\mathrm{P}_1 - \mathrm{P}_2|$, the deviations from the equilibrium state become non-negligible. According to equation (2.27), the magnitude of the capillary pressure is proportional to the inverse of the interface curvature radius. That is why the phase behavior of fluid mixtures is the most affected by capillary pressures in tight porous media.

2.1.2 Conventional Formulation for Stability Analysis

This section presents the conventional formulation for flash calculations. The algorithms used to solve the problems formulated below will be presented in Section 2.2.1.

2.1.2.1 Gibbs Free Energy

A stability analysis is a calculation performed to determine whether a hypothetical reference phase can minimize its Gibbs free energy by splitting into two or more phases at a given temperature, pressure, interfacial tension and composition. These calculations are convenient to perform using intensive variables which is why we introduce z_{i} and β_{j} as the mole fraction of component i the overall mixture (also called reference phase) and phase mole fraction of phase j in the overall mixture respectively. These variables along with x_{ij} are defined as fractions of molar quantities such that

$\sum_{i=1}^{N_c} x_{ij} = 1$, where $j = 1, \dots, N_p$,

$\sum_{j=1}^{N_p} \beta_j = 1$,

$\sum_{i=1}^{N_c} z_i = 1$, where $i = 1, \dots, N_c$.

The mole balance equation relates the composition of the reference mixture with that of the equilibrium phases such that

$z_i = \sum_{j=1}^{N_p} \beta_j x_{ij}$.

We also define the reduced molar Gibbs free energy $\underline{G}_R$ as a dimensionless intensive proxy variable for the total Gibbs free energy of a system such that

$$\underline{G}_R = (G - G^{IGM})/NRT = \sum_{j=1}^{N_p} \sum_{i=1}^{N_c} \beta_{ij} x_{ij} \ln(f_{ij}). \quad (2.28)$$

The stability problem can be formulated as the following. A mixture is stable if and only if there is no phase configuration for which the following condition is true:

$\sum_{j=1}^{N_p} \sum_{i=1}^{N_c} \beta_{ij} x_{ij} \ln(f_{ij}) \leq \sum_{i=1}^{N_c} z_i \ln(f_i)$

Baker et al. (1982) analyzed the Gibbs free energy of mixtures in composition space and proved that the tangent plane to the Gibbs free energy of a stable mixture must lie below the Gibbs free energy surface in composition space. In their analysis, Baker et al. (1982) assumed that the pressure of both the reference and incipient phases have the same pressure.

Michelsen (1982a) developed an algorithm for stability analysis to automatically assess the stability of a mixture based on the criterion of Baker et al. (1982). He defines the distance between the Gibbs free energy curve and the tangent plane to the Gibbs free energy of the reference phase as the Tangent Plane Distance (TPD) and uses a cubic equation of state to compute it. His procedure consists in computing the local minima of the TPD and evaluating its sign. If the TPD is negative for any composition, the mixture is unstable and splits into two or more phases at equilibrium.

The TPD can be derived as using a first-order Taylor series expansion of the reduced molar Gibbs free energy in equation (2.28) about the composition of the reference phase. The expression for the equation of the tangent plane can be simplified using the Gibbs-Duhem equation (2.7) to

$$T(\underline{x}) = \sum_{i=1}^{N_c} x_i \ln(f_{ir}), \tag{2.29}$$

where f_{ir} is the fugacity for component i ($i = 1, \dots, N_c$) in the reference phase. The TPD is then the difference between the Gibbs free energy and the tangent plane to the reference phase. Michelsen (1982a) originally assumed that both the reference phase and the incipient phase have the same pressure which canceled out the pressure terms in the fugacity. However, that assumption is invalid for tight reservoirs. A more general expression for the tangent plane distance function D evaluated at any pressure can then be derived as

$$D(\underline{\mathbf{x}}, P) = \sum_{i=1}^{N_c} x_i(\ln(f_i) - \ln(f_{ir})). \tag{2.30}$$

Michelsen's (1982a) method consists in computing the stationary points of D by numerically solving for the compositions at which the derivatives of D are equal to 0. The derivatives of D can be evaluated then simplified using the Gibbs-Duhem equations (2.7). The stationary condition is then

$$\partial D/\partial x_i = \ln(f_i) - \ln(f_{ir}) - \left(\ln(f_{N_c}) - \ln(f_{N_c r})\right) = 0, \text{ where } i = 1, \dots, N_c. \tag{2.31}$$

At the stationary point, D is equal to

$$D_{SP} = \ln(f_i) - \ln(f_{ir}), \text{ where } i = 1, \dots, N_c. \tag{2.32}$$

We can rearrange equation (2.31) using equation (2.32) in terms of a new variable $X_i = x_i e^{-D}$ such that

$$\ln(X_i P \phi_i) - \ln(f_{ir}) = 0, \text{ where } i = 1, \dots, N_c. \tag{2.33}$$

The variable P in equation (2.33) represents the pressure of a hypothetical incipient phase. An equivalent stability criterion at the stationary points to positivity of the TPD is then that

$$\mathrm{tD}(\mathbf{X}) = 1 - \sum_{i=1}^{N_c} X_i \geq 0. \tag{2.34}$$

The formulation for the stability problem is then the following:

Minimize $\mathrm{tD}(\mathbf{X})$ such that $\mathbf{X} > \mathbf{0}$.

The stability analysis above is formulated for a fixed capillary pressure. Since the capillary pressure is a function of equilibrium phase properties, it tends to be initially unknown. Therefore, stability analysis algorithms are often coupled with phase-split calculation algorithms to compute the equilibrium phase properties necessary to evaluate the capillary pressure.

The conventional formulation of Michelsen (1982b) for phase-split calculation is by solving the fugacity equations with no capillary pressure. It is straightforward to derive a more general case for constant capillary pressure. The problem is then formulated as follows:

Solve $x_{ij} P_j \phi_{ij} = x_{iN_p} P_{N_p} \phi_{iN_p}$, where $i = 1, \dots, N_c$ and $j = 1, \dots, N_p - 1$

subject to the material balance for a fixed overall composition, temperature and phase pressures.

2.1.2.2 Helmholtz Free Energy

In 1982, Michelsen suggested that the stability criterion based on the tangent plane distance of the Helmholtz free energy is equivalent to that of the Gibbs free energy (assuming negligible contributions from the interfaces) but not computationally competitive. He derives an expression for the tangent plane distance to the Helmholtz free energy in terms of the number of moles of each component and the volume. The equation

of the tangent plane to the reference phase of the Helmholtz free energy is given by a Taylor series expansion. After simplifications using the Gibbs-Duhem equation (2.7) for negligible interfacial work, the equation for the tangent plane becomes

$$T(\underline{\mathbf{n}}, V) = \sum_{i=1}^{N_c} n_i \overline{G}_{ir} - P_r V, \tag{2.35}$$

where $\underline{\mathbf{n}}$ and V represent the number of moles and volume of a hypothetical incipient phase. $\overline{G}_{ir}$ and P_r are the partial molar Gibbs free energy and pressure of the reference phase respectively. The expression for the tangent plane distance to the Helmholtz free energy is obtained by subtracting the expression for the Helmholtz free energy of a hypothetical incipient phase from that of the tangent plane. The stability criterion using the Helmholtz free energy is then

$$D(\underline{\mathbf{n}}, V) = \sum_{i=1}^{N_c} n_i(\overline{G}_i - \overline{G}_{ir}) - V(P_r - P) \geq 0, \tag{2.36}$$

where $\overline{G}_i$ and P are the partial molar Gibbs free energy and pressure of a hypothetical incipient phase.

Michelsen (1988) suggested that the stability problem can be solved by directly minimizing D in equation (2.36) by changing the number of moles while holding the volume of the reference phase constant. This formulation is equivalent to that of Nagarajan et al. (1991) who minimized a modified tangent plane distance function. The new function is equal to the tangent plane distance divided by the volume of the trial phase V, the ideal gas constant R and the temperature T. The denominator of this division is a positive scalar, therefore the positivity of this modified TPD is an equivalent stability criterion to the positivity of the original TPD in equation (2.36). Geometrically, this new TPD function can also be derived as the tangent plane distance function to the Helmholtz free energy divided by the total volume, the ideal gas constant, and the temperature of the reference phase. This modified stability criterion is written as

$$D(\underline{\mathbf{d}}) = \sum_{i=1}^{N_c} d_i(\ln(f_i) - \ln(f_{ir})) - (P - P_r)/RT \geq 0 \tag{2.37}$$

where d_i is the molar density of component i such that $d_i = n_i/V = x_i/\underline{V}$ $(i = 1, \dots, N_c)$.

The standard procedure for a stability test with the Helmholtz free energy consists in computing and evaluating the TPD at its local minima. The local minima of the TPD correspond to compositions at which the derivative of the TPD is equal to 0. Using the Gibbs-Duhem equation (2.7), this condition fulfilled at the local minima can be derived as

$$\partial D/\partial d_i = \ln(f_i) - \ln(f_{ir}) = 0, \text{ where } i = 1, \dots, N_c. \tag{2.38}$$

The TPD stability criterion at the stationary points can be derived using equations (2.37) and (2.38) as

$$D_{SP} = (P_r - P)/RT \geq 0. \tag{2.39}$$

Note that the stationary points of the TPD as described in equation (2.38) fulfills the first order condition of equality of the fugacity for equilibrium with the reference phase. According to equation (2.39), the difference in pressure between the reference phase pressure and that of the stationary points of this modified Helmholtz free energy TPD determines the value of the TPD at the stationary points.

The stability criteria presented in equations (2.36) and (2.37) does not account for the capillary pressure effects. Kou and Sun (2018) attempted to derive a stability criterion using the Helmholtz free energy for mixtures in tight porous media. However, as we will show in Section 2.2.2, their formulation was incorrect. In chapter 3, we present the correct formulation and implement it in a numerical algorithm for stability testing in tight porous media.

2.1.3 Cubic Equations of State

The procedures explained in the previous section described the basics for computing the thermodynamic state of a mixture in a system defined by $N_c + 2$ constraints. These procedures involved the computation of two primordial variables which are the fugacity of a component and the pressure of a phase for given values of the ideal gas constant, the temperature, the composition and either the volume or the pressure of the system. Given that all of those properties are non-linear functions of each other, they can be evaluated using correlations that can be tuned to experimental data. A correlation which can relate all of the properties aforementioned is called an equation of state. The simplest one is the ideal gas equation of state

$$P = NRT/V = RT/\underline{V}, \tag{2.40}$$

where $\underline{V}$ is defined as the molar volume of a mixture such that $\underline{V} = V/N$.

Equation (2.40) can be derived from statistical mechanics for a gas composed of point-particles of infinitesimal volume which do not interact with each other. Those two assumptions may only be valid at low temperatures and with electronically neutral particles such as noble gases. Due to these assumptions, the ideal gas equation of state cannot be used to model hydrocarbon liquid.

In 1873, van der Waals showed that two simple terms could be used to correct the ideal gas equation of state and improve its ability to model real fluids. The first correction consisted in adding a term to represent the electrostatic repulsion between particles at a very close distance due to the interaction of the electron clouds of two particles. This correction attributes a finite size to particles such that the total volume cannot be decreased below that occupied by the particles themselves. If the molar volume occupied by the particles is represented by the co-volume parameter b, the corrected ideal gas equation of state then becomes

$$P = RT/(\underline{V} - b). \tag{2.41}$$

One more correction applied to the ideal gas equation of state by van der Waals (1873) is to account for the interaction potential between particles at medium ranges. The inter-molecular interaction potential energy group of molecules is a function of the distance that separates them. For simplification purposes, we only consider the interaction between a pair of two molecules. The average distance between two molecules in a uniform substance is then related to its molar density. We assume that this correlation is related by a linear variable called the attraction parameter a. The complete form of the van der Waals equation of state can then be written as

$$P = RT/(\underline{V} - b) - a/\underline{V}^2. \tag{2.42}$$

The greatest advantage of the van der Waals EOS is able to predict liquid/vapor phase transitions as opposed to the ideal gas equation of state. The parameters a and b can even be rigorously determined by solving for the equality of the first and second isothermal derivatives of the pressure to 0 at the critical point for pure substances of known critical temperatures and pressures. This type of equation of state is called a cubic equation of state because the solution of the molar volume for a given pressure is that of a third-degree polynomial.

However, the volumetric and phase behavior predictions by the van der Waals equation of state are relatively inaccurate for most substances. This led to the development of modified versions of the van der Waals equation of state to fit the behavior of some specific chemical species. For example, the Peng-Robinson (1976; 1978) and Souave-Redlich-Kwong (1972) equations of state were designed to model the state of hydrocarbon mixtures at elevated pressures and temperatures and are still used in most reservoir simulators. In this research, we use the Peng-Robinson equation of state (PR EOS) only. It can be written as

$$P = RT/(\underline{V} - b) - a/(\underline{V}^2 + 2\underline{V}b - b^2), \quad (2.43)$$

where the specific expressions for the co-volume and attraction parameters are

$$a = 0.45724R^2T_c^2\alpha/P_c$$

$$b = 0.07780RT_c/P_c$$

$$\alpha = \left(1 + \kappa\left(1 - \sqrt{T/T_c}\right)\right)^{1/2}$$

$$\text{if } \omega < 0.49, \kappa = 0.37464 + 1.54226\omega - 0.26992\omega^2$$

$$\text{Otherwise, } \kappa = 0.379642 + \omega\left(1.48503 - \omega(0.164423 + 0.016666\omega)\right)$$

For multi-component mixtures, the PR EOS can be evaluated as a function of the critical properties of each chemical species and their interactions. The interactions can be modeled with mixing rules that compute the attraction and co-volume parameters for an equivalent pseudo-component describing the volumetric behavior of the mixture with equation (2.43). The most commonly used mixing rule for the PR EOS in reservoir engineering is the van der Waals mixing rules.

The mixture co-volume parameter b_m represents the volume occupied by hard-spheres particles per mole of substance. Therefore, it makes sense to calculate using a weighted linear average of the co-volume parameters for all the different chemical species present in the mixture.

$$b_m = \sum_{i=1}^{N_c} z_i b_i$$

The cubic EOS term containing the attractive parameter resembles most to the first virial coefficient term for which the mixing rules can be derived from statistical mechanics. That mixing rule consists of a geometric average of the attraction parameters of each species. In order to allow more flexibility for the EOS to fit experimental measurements of phase behavior, binary interaction parameters k_{ij} are introduced into this mixing rule. The van der Waals mixing rules then become

$$a_m = \sum_{i=1}^{N_c} \sum_{j=1}^{N_c} z_i z_j a_{ij},$$

where $a_{ij} = \sqrt{a_i a_j}\left(1 - k_{ij}\right)$ ($i = 1, \ldots, N_c$ and $j = 1, \ldots, N_c$). The matrix composed of binary interaction parameters (BIP) is symmetric, where the elements on the main diagonal are equal to 0.

Using equation (2.43), we can then evaluate the fugacity coefficient of a mixture.

$$\ln(\phi_i) = B_i/B_m(Z - 1) - \ln(Z - B_m) \qquad (2.44)$$
$$-A_m/(2\sqrt{2}B_m)\left(2\sum_{j=1}^{N_c} z_j A_{ij}/A_m - B_i/B_m\right)$$
$$\ln\left([Z + \left(1 + \sqrt{2}\right)B_m]/[Z + \left(1 - \sqrt{2}\right)B_m]\right)$$

where the capitulated terms A and B are dimensionless forms of a and b, and Z is called the compressibility factor.

$$A = aP/(RT)^2$$

$$B = bP/RT$$

$$Z = P\underline{V}/RT$$

The calculation of the fugacity coefficient requires the ability to solve the cubic EOS for the compressibility factor. By rearranging equation (2.43), we can express it as a cubic polynomial as a function of the compressibility factor.

$$Z^3 + (B - 1)Z^2 + (A - 3B^2 - 2B)Z + (B^3 + B^2 - AB) = 0 \qquad (2.45)$$

Equation (2.45) can be solved analytically using Cardano's method. It may have one to three real roots. In case it has more than one real root, the stable root with the lowest Gibbs free energy is selected. The stability of the root is determined by the positivity of the curvature of the Gibbs free energy curve or, equivalently by the negativity of the derivative of pressure with volume.

$$\partial^2 G/\partial\underline{V}^2 = -\partial P/\partial\underline{V} > 0 \qquad (2.46)$$

When there are three real roots, the middle root is always unstable and therefore consistently discarded. The correct remaining root can then be selected based on the second

law of thermodynamics. The most stable root is then that with the lowest Gibbs free energy for the two remaining roots Z_1 and Z_2. This selection criterion can be written as follows;

$$\text{if } \sum_{i=1}^{N_c} z_i(\ln(\phi_{i1}) - \ln(\phi_{i2})) \geq 0, \text{ use } Z = Z_1, \quad (2.47)$$

otherwise, use $Z = Z_2$.

2.1.4 IFT and Capillary Pressure Models

This section describes the numerical models used to evaluate the capillary pressure. The fundamental theories behind these correlations are also explained.

2.1.4.1 Parachor Model for IFT

We use the Parachor model to compute the fluid-fluid IFT. This model is based on the critical scaling theory and has been demonstrated to accurately model oil and gas mixture IFT by several authors (Weinaug and Katz, 1943; Lee and Chien, 1984; Schechter and Guo, 1998). It can be written as

$$\sigma^{LV} = \left(\sum_{i=1}^{N_c} \Pi_i(d_{iL} - d_{iV})\right)^{\gamma} \quad (2.48)$$

where Π_i and γ are the parachor coefficient for component i and the parachor exponent. The most recent estimate of the parachor exponent based on the most comprehensive dataset was done by Schechter and Guo (1998) who found it equal to 3.88. For most of our example cases we use this value as it is the most recent estimate based on the largest experimental dataset.

2.1.4.2 Young-Laplace Capillary Pressure

The Young-Laplace capillary pressure model assumes that the rock behaves as a bundle of tubes with chemically uniform surfaces and constant capillary radii $\mathcal{R}$. Figure 1 shows a schematic for this tube for a liquid-vapor (LV) equilibrium. The total fluid volume and the surface area for the boundary of the system are constant. The LV interfacial area is

not constrained and therefore contracts into a spherical shape as discussed in Section 2.1. At the three-interface-contact-line, the interfacial tension of each interface competes to minimize their respective areas. At equilibrium, the forces are balanced for a fixed angle θ. h represents the length of the tube occupied by the volume of vapor such that the total vapor volume is given by $V_V = \pi\mathcal{R}^2 h$ and the surface area of the tube in contact with vapor is given by $a_V = 2\pi\mathcal{R}h$. The volume of the vapor phase is given by $V_L = \pi\mathcal{R}^2(l - h)$, the boundary area in contact with the liquid phase is $a_L = 2\pi\mathcal{R}(l - h)$, and the liquid-vapor spherical interfacial area is $a_{LV} = \pi\mathcal{R}^2(1 + (\cos(\theta)^{-1} - 1)^2)$ where θ is the called the contact angle such that it is conventionally measured through the densest phase.

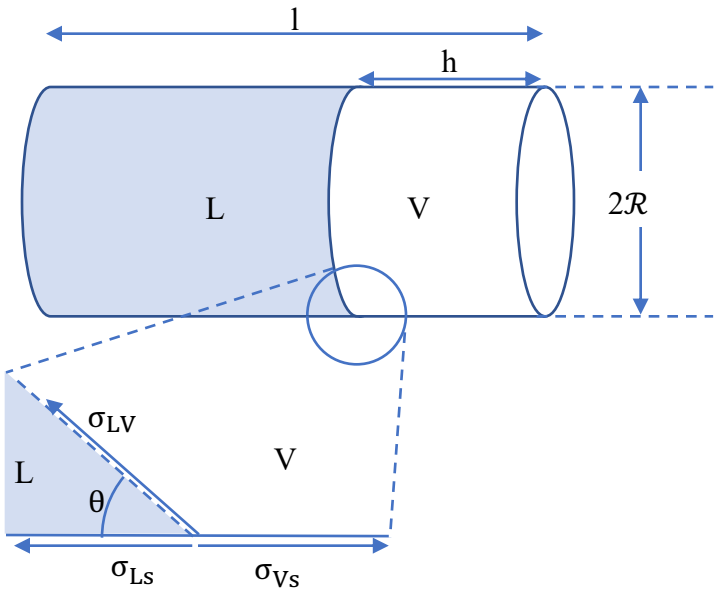

Figure 1: Schematic for curved liquid-vapor interphase in a uniform tube.

The Young-Laplace capillary pressure can then be derived from equation (2.22) and (2.23) for a liquid-vapor equilibrium. The derivatives in terms of vapor volume can be evaluated by using the chain rule to write them as a function of h. The term $\partial a_{VL}/\partial V_V$ is

0 because liquid-vapor interfacial area is not a function of h. Assuming that the vapor is less dense than the liquid phase, the capillary pressure then becomes

$$P_{cap} = P_V - P_L = (\sigma_{Vs} - \sigma_{Ls})(\partial a_{Vs}/\partial h)/(\partial V_V/\partial h) = 2(\sigma_{Vs} - \sigma_{Ls})/\mathcal{R}. \quad (2.49)$$

The force balance across the three-interface contact line gives the Young-Dupré equation

$$\cos(\theta) = (\sigma_{Vs} - \sigma_{Ls})/\sigma_{LV}. \quad (2.50)$$

The contact angle is a macroscopic property that is often used to characterize the preferential wettability of a solid surface. A surface preferentially wets a fluid if it can minimize the total energy of the system by increasing its surface area in contact with the wetting fluid at the expense of its area in contact with the non-wetting fluid. Most reservoir rocks are preferentially oil-wet because $\sigma_{Vs} > \sigma_{Ls}$. As the vapor phase is usually less dense than the liquid phase $\cos(\theta)$ is generally positive for hydrocarbon reservoir rocks. Equations (2.49) and (2.50) give the expression for the Young-Laplace capillary pressure

$$P_{cap} = 2\sigma_{LV}\cos(\theta)/\mathcal{R}. \quad (2.51)$$

The main assumption for modeling the capillary pressure in a porous medium with the Young-Laplace model is that the pores act like a bundle of smooth capillary tubes of average capillary radius $\mathcal{R}$ as shown in the schematic below.

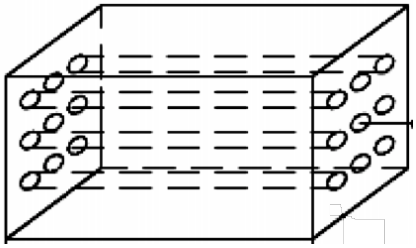

Figure 2: Schematic (Al-droury, 2010) for the bundle of tubes used as an approximation for modeling capillary pressure in a porous medium with the Young-Laplace model.

In the literature, the Young-Laplace model is the most frequently used for modeling the impact of capillary pressure on phase behavior. That model does not represent real the

physics of rocks which have heterogeneous wettability and complex pore structure. The wettability of the rock surface at the interface and the capillary radius of the pore in which it is confined are too unpredictable to be used with a Young-Laplace model.

2.1.4.3 Saturation-Based Capillary Pressure

Saturation-based capillary pressure models take into account the complexity of the pore size distribution through measurable parameters that characterize the bulk rock properties. Figure 3 presents a schematic for the type of complex interface geometry that can be modeled with empirical saturation-based capillary pressure. The fluid and rock-dependent properties can be scaled with Leveret J-type functions. A saturation-based model which takes into account the presence of water on the oil/gas capillary pressure was presented by Neshat et al. (2018)

$$\mathrm{P^{cap}}(\mathrm{S_o}) = \sigma_{\mathrm{LV}}\sqrt{\phi/\mathrm{k}}\left(b_{\mathrm{o}}/(\mathrm{S_o}+\mathrm{S_w})^{a_{\mathrm{o}}} + b_{\mathrm{g}}/\left(\mathrm{S_g}\right)^{a_{\mathrm{g}}}\right) \tag{2.52}$$

where ϕ and k are respectively the porosity and the permeability of the porous medium, and a_{o}, b_{o}, a_{g}, and b_{g} are fitting parameters which allow the user to fit the model to experimentally measured capillary pressure data.

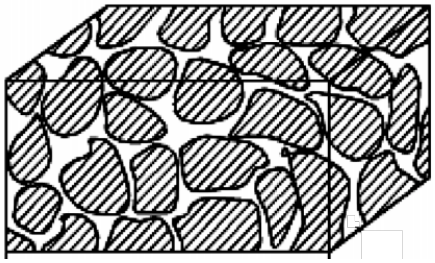

Figure 3: Schematic (Al-droury, 2010) for the complex pore structure of reservoir rocks that can be modeled using saturation-based capillary pressure.

One aspect of these saturation based capillary pressure models is that they increase asymptotically near residual saturations. In order to avoid calculating infinite capillary pressures, Neshat at al. (2018) suggested using a maximum value corresponding to the

Young-Laplace capillary pressure at the minimum measurable pore-size $\mathcal{R}_{\min}$. The maximum pore size $\mathcal{R}_{\max}$ can also be used to limit the minimum value of the capillary pressure. Hence the oil saturations used for capillary pressure vary from S_{omin} to $1 - S_{gmin}$ where $P^{cap}(S_{omin}) = 2/\mathcal{R}_{\min}$ and $P^{cap}(S_{gmin}) = 2/\mathcal{R}_{\max}$.

2.1.5 Basics of Minimization and Equation Solving Algorithms

In this report, stability analysis is carried out using numerical algorithms to compute the global minima of various functions based on the Gibbs free energy and the Helmholtz free energy. As global minimization algorithms tend to be very computationally expensive, equilibrium calculations in reservoir simulators use local minimization routines with multiple initial guesses. This computation can be performed by using either minimization algorithms to compute all the local minima, or by using equation solving methods to compute all the stationary points.

In this report, linearly constrained minimization problems are formulated in the following way:

Minimize $F(\mathbf{x})$,

such that $\mathbf{a} < \mathbf{A}\mathbf{x} < \mathbf{b}$,

and $\mathbf{x} \in \mathbb{R}^N$.

Gradient-based local minimization algorithms require that F be a twice differentiable function of $\mathbf{x}$, where $\mathbf{x}$ is a vector of N independent variables. $\mathbf{x}$ is constrained such that the value its linear product the matrix $\mathbf{A}$ is within the range $(\mathbf{a}, \mathbf{b})$. The local minima of F at $\mathbf{x}_{SP}$ are defined by the conditions that $\boldsymbol{\nabla} F(\mathbf{x}_{SP}) = \mathbf{0}$, and $\boldsymbol{\nabla}^2 F(\mathbf{x}_{SP})$ is positive definite.

In this research, we use local minimization methods which iteratively update the independent variable $\mathbf{x}$ until it satisfies the stationarity condition $\boldsymbol{\nabla} F(\mathbf{x}_{SP}) = \mathbf{0}$. The

general iterative scheme for updating the independent variable $\mathbf{x}$ is $\mathbf{x}^{k+1} = \mathbf{x}^k + \lambda \boldsymbol{d}^k$, where $\boldsymbol{d}^k$ is the step direction which determines the direction of the variable update of $\mathbf{x}^k$. Gradient-based method generally estimate the direction of an iterative update as $\boldsymbol{d}^k = -\mathbf{C}\boldsymbol{\nabla}\mathrm{F}(\mathbf{x}^k)$. The two methods considered in this research are the gradient descent method where $\mathbf{C}$ is the identity matrix and the Newton-Raphson method where $\mathbf{C}$ is the inverse of the Hessian matrix of F at $\mathbf{x}^k$. λ is the scalar step-size which determines the magnitude of the change of the iterative update of the variable $\mathbf{x}^k$.

The gradient descent method can be derived by approximating F with a first-order Taylor series expansion

$$\mathrm{F}(\mathbf{x}^k + \lambda \boldsymbol{d}^k) = \mathrm{F}(\mathbf{x}^k) + \lambda \boldsymbol{d}^k \boldsymbol{\nabla}\mathrm{F}(\mathbf{x}^k) + o(||\lambda \boldsymbol{d}^k||^2), \tag{2.53}$$

where $o(||\lambda \boldsymbol{d}^k||^2)$ represents the remaining terms of the Taylor series' expansion which scales as a function of the magnitude of $||\lambda \boldsymbol{d}^k||^2$. For a fixed norm of the vector $\boldsymbol{d}^k$, equation (2.53) can be rearranged to give

$$\Delta\mathrm{F} = \mathrm{F}(\mathbf{x}^k + \lambda \boldsymbol{d}^k) - \mathrm{F}(\mathbf{x}^k) = \lambda |\boldsymbol{d}^k| |\boldsymbol{\nabla}\mathrm{F}(\mathbf{x}^k)| \cos(\varpi), \tag{2.54}$$

where ϖ is the angle between the vectors $\boldsymbol{d}^k$ and $\boldsymbol{\nabla}\mathrm{F}(\mathbf{x}^k)$. For a fixed norm of the vector $\lambda \boldsymbol{d}^k$, $\Delta\mathrm{F}$ is minimized at $\varpi = \pi$. This direction of $\boldsymbol{d}^k$ corresponding to that angle is then $\boldsymbol{d}^k = -\boldsymbol{\nabla}\mathrm{F}(\mathbf{x}^k)$. Gradient descent methods use the gradient to compute the direction of the steepest descent of the objective function and generally need a method of determining how long the step-size should be.

Newton's method can be derived by approximating the objective function with a second-order Taylor-series approximation as

$$\mathrm{F}(\mathbf{x}^k + \boldsymbol{d}^k) = \mathrm{F}(\mathbf{x}^k) + \boldsymbol{d}^k \boldsymbol{\nabla}\mathrm{F}(\mathbf{x}^k) + 1/2(\boldsymbol{d}^k)^{\mathrm{T}} \boldsymbol{\nabla}^2 \mathrm{F}(\mathbf{x}^k)(\boldsymbol{d}^k) + o(||\lambda \boldsymbol{d}^k||^3) \tag{2.55}$$

where $o(||\lambda \boldsymbol{d}^k||^3)$ is the residual term to be neglected. At a local minimum of F near $\mathbf{x}^k$, the gradient is equal to 0. The gradient of F in equation (2.55) at the local minimum is

$$\nabla \mathrm{F}\left(\mathbf{x}^{\mathrm{k}}+\boldsymbol{d}^{\mathrm{k}}\right)=\nabla \mathrm{F}\left(\mathbf{x}^{\mathrm{k}}\right)+\boldsymbol{d}^{\mathrm{k}} \nabla^{2} \mathrm{F}\left(\mathbf{x}^{\mathrm{k}}\right)=\mathbf{0}, \text{ which gives} \tag{2.56}$$

$$\boldsymbol{d}^{\mathrm{k}}=-\nabla^{2} \mathrm{F}\left(\mathbf{x}^{\mathrm{k}}\right)^{-1} \nabla \mathrm{F}\left(\mathbf{x}^{\mathrm{k}}\right) \tag{2.57}$$

The pure Newton's method provides a guess for the optimal step-size assuming that the function is near-quadratic. This assumption is correct for small the residuals $o(||\lambda \boldsymbol{d}^{\mathrm{k}}||^{3})$ of the Taylor series approximation on the order of $||\lambda \boldsymbol{d}^{\mathrm{k}}||^{3}$. For small values of $\boldsymbol{d}^{\mathrm{k}}$, the residual is negligible, and the convergence behavior is said to be quadratic. However, it is necessary to adjust the step size when the magnitude of $||\lambda \boldsymbol{d}^{\mathrm{k}}||^{3}$ is "large" or when the objective function F at $\mathbf{x}^{\mathrm{k}}$ is "far" from the local minimum.

The method used to determine the optimal step-size for the iterative update in the gradient-descent method and the Newton-Raphson method is called line-search. This is consists in the following optimization.

Minimize $\mathrm{F}\left(\mathbf{x}^{\mathrm{k}}+\lambda \boldsymbol{d}^{\mathrm{k}}\right)$,

such that $\lambda \in (0, \mathrm{s})$ and $\mathbf{x}^{\mathrm{k}}$ and $\boldsymbol{d}^{\mathrm{k}}$ are constants.

The step-size λ must be positive in order to maintain the direction of the update vector. A maximum value s can also be set to avoid the step-size being too long. For the Newton-Raphson method, s is commonly set to be 1. In the case where the value of $\mathrm{s}=1$ violates the constraints on $\boldsymbol{d}$, s can be reset such that the independent variable remains in the defined domain.

Newton's method can also fail if $\mathbf{x}^{\mathrm{k}}$ corresponds to a point on F at which F is not convex. In that case, the direction computed by Newton's method $\boldsymbol{d}^{\mathrm{k}}$ points towards a saddle point or local maximum of F. The modified Cholesky decomposition (Gill and Murray, 1974) is then a commonly used method to adjust the Hessian matrix $\nabla^{2} \mathrm{F}\left(\mathbf{x}^{\mathrm{k}}\right)$ to force it to become positive-definite. Additionally, near singular Hessian matrices may result in the overestimation of the Newton-Raphson step sizes (Dennis and Schnabel, 1996). A variant of the modified Cholesky decomposition (Dennis and Schnabel, 1996) can then

be used to adjust the direction vector when the Hessian is not sufficiently positive-definite as well.

An alternative method for computing the local minima of a function is by directly solving the stationarity equation. The stationarity equation defines all the extrema of a function at which the gradient of that function is evaluated to be 0. The formulation for an equation solving method can be written as follows.

Solve the system of equations $\mathcal{F}_{\mathrm{i}}(\mathbf{x}) = 0$,

where $\mathrm{i} = 1, \ldots, \mathrm{N}$, and $\mathcal{F}: \mathbb{R}^{\mathrm{N}} \to \mathbb{R}^{\mathrm{N}}$.

The Newton-Raphson method can also be used as an equation-solving method as well. This numerical method consists in iteratively update the independent variable

$$\mathbf{x}^{\mathrm{k}+1} = \mathbf{x}^{\mathrm{k}} + \alpha(\boldsymbol{\nabla}\boldsymbol{\mathcal{F}})\boldsymbol{\mathcal{F}},$$

where $\boldsymbol{\nabla}\boldsymbol{\mathcal{F}}$ is called the Jacobian matrix of $\boldsymbol{\mathcal{F}}$. For the special case where $\boldsymbol{\nabla}\boldsymbol{\mathcal{F}}$ is a symmetric matrix, there exists a scalar function $\mathrm{F}(\mathbf{x})$ such that $\boldsymbol{\nabla}\mathrm{F} = \boldsymbol{\mathcal{F}}$. The root finding method then reverts to the Newton-Raphson minimization algorithm, such that the Jacobian of $\boldsymbol{\mathcal{F}}$ is the Hessian of F.

The fixed-point iteration method can also be used to solve a system of equations. This method can be used only if the system of equation is linearizable as a function of the independent variable $\mathbf{x}$ and a new function $\boldsymbol{\mathcal{G}}(\mathbf{x})$ such that

$$\boldsymbol{\mathcal{F}} = \mathbf{x} + \boldsymbol{\mathcal{G}}(\mathbf{x}).$$

The variable $\mathbf{x}$ can then be iteratively updated until the system of equations $\boldsymbol{\mathcal{F}} = \mathbf{0}$ is solved.

$$\mathbf{x}^{\mathrm{k}+1} = \boldsymbol{\mathcal{G}}\left(\mathbf{x}^{\mathrm{k}}\right)$$

2.2 LITERATURE REVIEW

This section presents various stability analysis algorithms which were designed for hydrocarbon liquid/vapor systems. First, a review of conventional flash calculation algorithms using Gibbs free energy is presented. Next, we present an overview of some methods for stability analysis using the Helmholtz free energy.

2.2.1 Stability Analysis Using the Gibbs Free Energy

The previous sections derived the formulations for equilibrium calculations using Gibbs free energy. This section presents the conventional flash calculation algorithms developed by Michelsen (1982a; 1982b). Next, it discusses how the conventional methods for phase-split and stability analysis algorithms were coupled with capillary pressure models to analyze the stability of mixtures in tight porous media.

2.2.1.1 Conventional Algorithms for Flash Calculation

Both traditional algorithms for phase-split and phase-stability calculations use a fixed-point iteration method called successive substitution (SS). SS is widely used because of its simplicity and robustness. It was presented by Michelsen (1982a; 1982b) to model the equilibrium state of hydrocarbon mixtures in reservoirs with negligible capillary pressures.

The phase-split calculation uses the K-values as the independent variable such that

$$K_{ij} = x_{ij}/x_{iN_p}, \text{ where } i = 1, \dots, N_c \text{ and } j = 1, \dots, N_p - 1. \tag{2.58}$$

K-values are also called partition coefficients because their magnitude characterizes how much of each individual component partitions in each phase. For a negligible capillary pressure, the fugacity equation (2.14) can be rearranged to obtain a fixed-point iteration independent variable update equation

$$\ln\left(K_{ij}^{k+1}\right) = \ln\left(\phi_{iN_p}^{k}\right) - \ln\left(\phi_{ij}^{k}\right), \text{ where } i = 1, \dots, N_c, j = 1, \dots, N_p - 1, \tag{2.59}$$

where the subscripts k indicate the iteration step at which the variable is evaluated.

According to equation (2.44), the fugacity coefficients in equation (2.59) can be calculated as a function of the phase composition, pressure, and temperature. Therefore, it is necessary to compute the compositions of each phase for a given set of K-values and overall composition. This is a standard procedure commonly called constant K-flash calculation as originally proposed by Rachford and Rice (1952). The problem consists in solving the Rachford-Rice equations

$$f_j(\boldsymbol{\beta}) = \sum_{i=1}^{N_c}(1 - K_{ij})z_i/t_i = 0, \text{ where } j = 1, \dots, N_p - 1, \quad (2.60)$$

such that $x_{ij} \geq 0$, where $i = 1, \dots, N_c$ and $j = 1, \dots, N_p$

t_i is a constant defined as $t_i = 1 - \sum_{j=1}^{N_p-1}(1 - K_{ij})\beta_{ij}$ $(i = 1, \dots, N_c)$.

Many algorithms have been developed to solve this problem (Michelsen, 1994; Leibovici and Neoschil, 1995; Okuno et al., 2010) as summarized by Okuno (2009). In the research, we use the method of Okuno et al. (2010) for its robustness and efficiency. It solves the Rachford-Rice equations as a minimization problem of the following globally convex function

$$F(\boldsymbol{\beta}) = \sum_{i=1}^{N_c} -z_i \ln(t_i).$$

The K-flash calculation is then formulated as a minimization problem the Jacobian of the Rachford-Rice equations is a symmetric Hessian $\boldsymbol{\nabla}^2 F(\boldsymbol{\beta}) = \mathbf{H}$ defined as

$$H_{jk} = \sum_{i=1}^{N_c}(1 - K_{ij})(1 - K_{ik})z_i/t_i^2, \text{ where } j = 1, \dots, N_p - 1 \text{ and } k = 1, \dots, N_p - 1$$

The feasible domain of $\boldsymbol{\beta}$ is defined by the non-negativity of the component phase mole fractions. Mathematically, this condition translates into the following set of constraint equations:

$\mathbf{A\beta} \leq \mathbf{b}$, where $A_{ij} = 1 - K_{ij}$ and $b_i = \min(1 - z_i, \min(1 - K_{ij}z_i))$

Okuno et al. (2010) also formulated a line-search method to optimize the step-size of the Newton update. Although this section of the algorithm was implemented, it is not

needed to guarantee the convergence of the algorithm since the initial guess is in general rather close to the solution where the assumption of near quadraticity is valid.

The K-flash algorithm consists of the following steps.

Step 1. Generate an initial estimate for the independent variables $\boldsymbol{\beta}$ $\left(\mathrm{j} = 1, \dots, \mathrm{N_p} - 1\right)$ based on an equally weighted mean of the vertices of the feasible region.

Step 2. Calculate the gradient and the Hessian of the convex function F.

Step 3. Solve the system of linear equations for Newton's direction.

Step 4. Compute the maximum feasible step-size $\lambda_{\max}$

$\lambda_{\max} = \min((\mathrm{b_i} - \mathbf{A_i} \cdot \boldsymbol{\beta})/(\mathbf{A_i} \cdot \boldsymbol{d}) : \mathbf{A_i} \cdot \boldsymbol{d} > 0)$

where $\mathbf{A_i}$ is a vector representing the i-th column in matrix $\mathbf{A}$.

Step 5. If $\lambda_{\max} \leq 1$, set the step-size to $\lambda = \mathrm{u}\lambda_{\max}$ where u is a specified underrelaxation factor. Otherwise, set the step-size to $\lambda = 1$.

Step 6. Update the independent variables $\boldsymbol{\beta}^{\mathrm{k+1}} = \boldsymbol{\beta}^{\mathrm{k}} + \boldsymbol{d}^{\mathrm{k}}\lambda$.

Step 7. If the maximum norm of the gradient is less than a specified tolerance $\varepsilon_{\mathrm{RR}}$, stop. Otherwise, continue to step 7.

Step 8. Increase the iteration index $\mathrm{k} = \mathrm{k} + 1$ and return to step 3.

The phase-split calculation algorithm can be initiated either by Wilson's correlation (1969) or using the stationary point composition of the tangent plane distance. Wilson's correlation provides estimations for the vapor pressure of hydrocarbon substances.

$$\mathrm{P_i^{vap}} = \mathrm{P_{ci}} \exp\left(5.37(1 + \omega_i)(1 - \mathrm{T_{ci}}/\mathrm{T})\right) \tag{2.61}$$

Assuming that the liquid phases behave as ideal solutions and that the gas phases behaves as ideal gas mixtures, Raoult's law can be used to estimate the K-values

$$\mathrm{K_i} = \mathrm{x_{iV}}/\mathrm{x_{iL}} \cong \mathrm{P_i^{vap}}/\mathrm{P} \tag{2.62}$$

This initial guess is only valid for hydrocarbon two-phase liquid/vapor equilibrium. For more general multi-phase equilibrium calculations, the initial guess K-values can be computed using the composition of the stationary points $\mathbf{x}_{\mathrm{SP}}$ to the TPD and the composition of the phase indexed $\mathrm{N_p}$ from the previous phase-split calculation

$$\mathrm{K_{i,N_p-1}} = \mathrm{x_{iSP}}/\mathrm{x_{iN_p}}. \tag{2.63}$$

The steps for the phase-split calculation using the SS method is then the following.

Step 1. Compute the initial guess for $\mathrm{N_c}\left(\mathrm{N_p}-1\right)$ K-values.

Step 2. Calculate the phase mole fractions and phase compositions using a constant K-flash calculation.

Step 3. Solve the cubic EOS for the compressibility factor and compute fugacity coefficients for $\mathrm{N_p}$ phases and $\mathrm{N_c}$ components.

Step 4. If the maximum norm of the fugacity equations vector is less than a specified tolerance $\varepsilon_{\mathrm{PS}}$, stop.

Step 5. Use equation (2.59) to update the K-values.

Step 6. Return to step 2.

The SS algorithm for phase-split calculations generally converges more slowly than Newton-Raphson based methods near the solution, however it is more robust. That is why most of the published methods for equilibrium calculations of hydrocarbon mixtures in tight porous media use SS. The robustness of the SS method is related to the fact that it can also be derived as a gradient descent method as shown by Mehra et al. (1983) using the K values as the independent variables. This is proven by using a variable transformation from the traditional local iterative minimization algorithm for the Gibbs free energy

$$\boldsymbol{d}_{\mathrm{lnK}} = \mathbf{U}\boldsymbol{d}_{\mathrm{n}} = -\mathbf{U}\mathbf{C}_{\mathrm{n}}\boldsymbol{\nabla}\mathrm{G}, \tag{2.64}$$

where $\boldsymbol{d}_{\mathrm{lnK}}$ and $\boldsymbol{d}_{\mathrm{n}}$ are the direction vectors for the minimization of G with the independent variables $\ln(\mathbf{K})$ and $\underline{\mathbf{n}}$ respectively. $\mathbf{U}$ is the transformation matrix used to convert the

gradient of the Gibbs free energy in the $\underline{\mathbf{n}}$ variable space to a gradient in the $\ln(\mathbf{K})$ variable space such that it contains the terms $\partial \ln(K_{ij}) / \partial N_{kl}$, $(i = 1, \dots, N_c, k = 1, \dots, N_c, j = 1, \dots, N_p - 1, l = 1, \dots, N_p - 1)$. $\mathbf{C}_n$ is the general coefficient matrix for gradient-based methods in the $\underline{\mathbf{n}}$ variable space. Equation (2.64) can then be rewritten as the general expression for the variable update direction in the $\ln(\mathbf{K})$ variable space $\boldsymbol{d}_{\ln K} = \mathbf{C}_{\ln K} \boldsymbol{\nabla} G$, where $\mathbf{C}_{\ln K} = \mathbf{U}\mathbf{C}_n$. If we set the matrix $\mathbf{C}_{\ln K}$ to the identity matrix and the step-size to 1, we get the following independent variable update equation for the gradient descent method

$$\ln(\mathbf{K})^{k+1} = \ln(\mathbf{K})^{k} - \boldsymbol{\nabla} G,$$

which is identical to the SS equation. Since the gradient descent method computes the direction of the update based on the maximum direction of descent of the objective function, it does not converge to saddle points. The convergence radius also tends to be larger than Newton-Raphson methods.

In Section 2.1.1.1, the formulation for stability analysis based on the Gibbs free energy TPD is presented. The method of Michelsen (1982a) consists in computing the global minimum of the Gibbs free energy TPD by using local minimization routines with multiple initializations. In order to locate all the local minima of the TPD function efficiently, Michelsen (1982a) proposed using the approximate K-values from Wilson's correlation with equations (2.61) and Raoult's law with equation (2.62) to generate two initial guesses for liquid-like X_{iL} and gas-like X_{iV} independent stability analysis variables, where

$$X_{iL} = z_i / K_i \text{ and} \tag{2.65}$$

$$X_{iV} = z_i K_i.$$

For multi-phase systems involving an aqueous phase or a second hydrocarbon liquid phase, other initialization methods have been proposed (Michelsen, 1982a; Firoozabadi and Li, 2012). Since multi-phase equilibrium calculations are out of the scope

of this report, only the two-phase initial guesses of Michelsen (1982a) are used in this research.

The numerical search for local minima can result in four possible outcomes. It can converge to the trivial solution where the composition of the hypothetically incipient phase is equal to that of the reference phase. At the trivial solution, the value of the TPD is 0, and therefore it does not provide any useful information about the stability of a phase. The local minimization can also converge to a non-trivial solution at which the TPD is positive. If all trial phases converge to either this kind of stationary point or to the trivial solution, then the mixture is stable. On the other hand, if one of the initial guesses converges to a non-trivial solution with a negative TPD, then the mixture is unstable and splits into two or more phases at equilibrium. In this case, the converged composition with the lowest TPD can be used to initiate the phase-split calculation. The fourth possible outcome is that the algorithm does not converge within the set maximum number of iterations. In this case, the stability analysis can be interrupted, and the value of the TPD at convergence can be used to evaluate the stability of the reference phase.

The equation for the variable update of the standard SS algorithm for stability analysis can be derived by rearranging stationarity condition equation (2.33) for the Gibbs free energy TPD as

$$X_i^{k+1} = z_i \phi_{ir} / \phi_i^k, \text{ where } i = 1, \dots, N_c. \tag{2.66}$$

The SS algorithm for stability analysis is then the following:

1. Compute the initial guesses for the trial phase composition.
2. Compute the compressibility factors by solving the cubic EOS (2.45). Compute the fugacity coefficient for the reference phase using equation (2.44). If necessary, select the correct root based on criterion (2.47).

3. Compute the initial trial phase compositions based on Wilson's correlation using equations (2.61), (2.62), and (2.65).
4. Compute the composition of the trial phase $x_i = X_i / \sum_{i=1}^{N_c} X_i$.
5. Compute the compressibility factors and fugacity coefficients for the trial phase.
6. If the maximum norm of set of equations (2.33) is less than a specified tolerance ε_{GS}, stop. Otherwise, continue to step 7.
7. Update the independent variables **X** using equation (2.68).
8. Return to step 3.

This SS algorithm for stability analysis is also linearly convergent. It is therefore slower than Newton-Raphson minimization algorithms. However, it is more robust because it is significantly less sensitive to the proximity of the initial guess to the solution. Most of the published methods for stability analysis in tight reservoirs focus on the robustness of the method which is why they tend to rely on the robustness of the SS algorithm.

2.2.1.2 Stability Analysis for Tight Reservoirs

The previous section presented the standard flash calculation equilibrium algorithms for negligible capillary pressures. This section discusses the challenges and solutions for implementing the capillary pressure effects into stability analysis algorithms for hydrocarbon mixtures in tight reservoirs.

It is straight-forward to include the capillary pressure in the algorithms for the independent variable update equation of both SS algorithms. For phase-split calculation, the K-values update equation can be rederived from the fugacity equation (2.14) for a non-equal phase pressure as

$$\ln\left(K_{ij}^{k+1}\right) = \ln\left(P_{N_p}\phi_{iN_p}^{k}\right) - \ln\left(P_j\phi_{ij}^{k}\right), \text{ where } i = 1, \dots, N_c \text{ and } j = 1, \dots, N_p - 1. \quad (2.67)$$

The independent value update equation for the stability analysis can be derived from the stationarity condition equation (2.33)

$$X_i^{k+1} = f_{ir}/P\phi_i^k, i = 1, \dots, N_c. \quad (2.68)$$

The stability criterion at the stationary point is expressed by equation (2.34).

Shapiro and Stenby (2001) analyzed phase equilibrium at high capillary pressure and pointed out two main differences with equilibrium at negligible capillary pressure.

1. In the case with no capillary pressure, both phases are always on the limit of stability of the Gibbs free energy curve. However, when capillary pressure is considered, the higher-pressure phase is always stable while the lower-pressure phase is always meta-stable. That is, the Gibbs free energy of the lower-pressure phase is between the stability limit and the spinodal boundary defined by a point of inflection on the Gibbs free energy surface.
2. For capillary pressures higher than that at the spinodal boundary, there is no equilibrium solution.

Rezaveisi et al. (2018) illustrated graphically the lack of a solution to capillary equilibrium and the validity of the TPD stability criterion for binary mixtures. Binary mixtures are often used for analyzing and understanding equilibrium because the Gibbs free energy curve at a fixed temperature and pressure can be represented on a 2-dimension plot. Their analysis is reproduced below with a binary mixture of methane and butane. The critical phase properties used to compute the Gibbs free energy for this mixture are listed in Table 1.

Component	T_c (K)	P_c (bar)	ω	BIP C_1	n-C_4
C_1	190.7	46.0	0.008	0	0
n-C_4	425.2	38.0	0.193	0	0

Table 1: Critical properties for methane/n-butane mixture

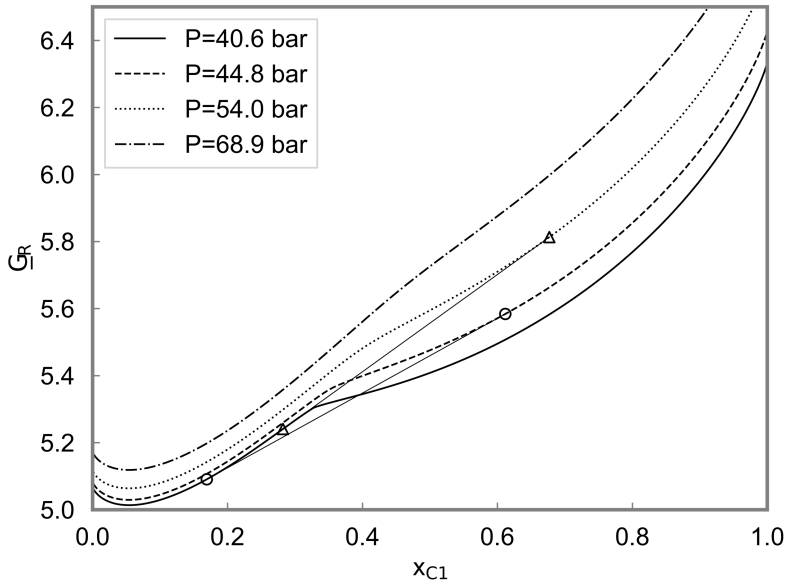

Figure 4: Gibbs free energy curves for C_1/n-C_4 mixtures at 361.1 K at 40.6, 44.8, 54.0, and 68.9 bar with tangent lines connecting equilibrium phase compositions.

Figure 4 shows the reduced dimensionless Gibbs free energy for hypothetical single-phase mixtures of methane (C_1) and n-butane (n-C_4) at 40.6, 44.8, 54.0, and 68.9 bar. The temperature used for all the cases is 361.1 K. For binary mixtures, a two-phase solution can be graphically determined by the existence of a common tangent line to the Gibbs free energy curves of the equilibrium liquid and vapor phase. In Figure 4, a common tangent line connects two equilibrium phases marked by hollow circles. The liquid phase pressure and composition are 40.6 bar and 17 mol% methane. The equilibrium gas phase pressure and composition are 44.8 bar and 61 mol% methane. A second common tangent line (Gibbs free energies are marked by hollow triangles) connects equilibrium phases for

a higher capillary pressure. As derived by Shapiro and Stenby (2001), the liquid phase composition moves away from the limit of stability to 28 mol% methane into the meta-stable region of the Gibbs free energy. The gas phase methane mole fraction increased to 68 mol% in the direction of the stable region of the Gibbs free energy. The second equilibrium liquid phase is on an inflection point of the Gibbs free energy curve. Therefore, its equilibrium capillary pressure defines the maximum value beyond which there is no equilibrium solution. Indeed, there is no common tangent line which can be drawn between the Gibbs free energy curve of the liquid phase at 40.6 bar and a hypothetical gas phase at 68.9 bar. Rezaveisi et al. (2018) concluded that the absence of an equilibrium solution indicates the mixture is stable.

Then, Rezaveisi et al. (2018) showed that mixtures can still have negative TPD even though they do not have an equilibrium solution. Figure 5 shows the TPD for methane/n-butane mixtures for a reference phase of 70 mol% methane at 68.9 bar. As we saw previously, this mixture has no equilibrium solution with a liquid phase of 40.6 bar. However, the tangent plane distance is negative for compositions of methane greater than 12 mol%. In this case, the TPD stability criterion disagrees with the stability criterion based on the existence of an equilibrium solution. Rezaveisi et al. (2018) concluded that the Gibbs free energy tangent plane distance criterion is invalid for high capillary pressures.

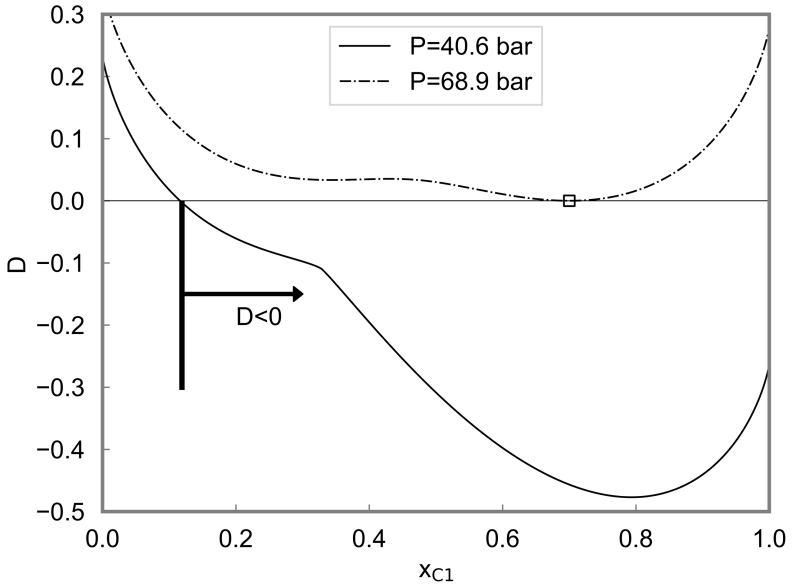

Figure 5: Gibbs free energy TPD curves for C_1/n-C_4 mixtures at 361.1 K at 40.6 and 68.9 bar. The reference phase contains 70 mol% methane at 68.9 bar.

Siripatrachai et al. (2017) used phase-split calculations to determine the stability of mixtures in order to avoid the potential failures of TPD-based algorithms described by Rezaveisi et al. (2018). Their phase-split algorithm uses the SS method with an iterative update of the capillary pressure using the Young-Laplace model. They use the phase-mole fraction at convergence to determine the stability of the reference phase. However, phase-split calculations often have no solution outside the phase envelope and can even diverge when the initial guess of the K-values is not accurate enough. These two vital issues make the use of phase-split calculations as a stability test not robust and unreliable for use in a reservoir simulator.

Sherafati and Jessen (2017) disregarded the claim of Rezaveisi et al. (2018) that the TPD criterion is invalid and compared the stability analysis using SS with other accelerated methods. Sherafati and Jessen (2017) only use relatively large capillary radii to avoid cases of negative TPD which lack an equilibrium solution at high capillary pressures. Sherafati

and Jessen (2017) iteratively update capillary pressure using the Young-Laplace model as a function of the trial and reference phase properties. In their derivation of the formulation, they neglect the derivatives of the capillary pressure with composition to force the TPD at the stationary point to be equal to 0 for an equilibrium phase. However, they do not give a valid physical explanation as to why that term should be neglected. This issue is addressed in the context of a new stability analysis algorithm that uses the Helmholtz free, energy instead of the Gibbs free energy, in Chapter 3.

Neshat et al. (2019) analyzed the Gibbs free energy and the TPD for hydrocarbon mixtures in tight reservoirs to determine the fundamental conditions under which the TPD criterion is valid for determining stability. Their analysis is demonstrated with the Gibbs free energy curves for an equimolar mixture of methane (C_1) and n-decane (n-C_{10}) as represented by point A in Figure 6. Table 2 shows the critical properties of this mixture. The temperature is 560.9 K and the reference pressure is 22.3 bar. The capillary pressure used for this stability analysis is 7.7 bar. The reference phase is in equilibrium with an oleic phase of 7.88 mol% methane and at 14.6 bar. The Gibbs free energy curve is shown by the solid line for the reference gas phase and by the dashed line for the oleic phase. Points A and B represent the reference and incipient phases respectively.

Component	T_c (K)	P_c (bar)	ω	BIP C_1	n-C_{10}
C_1	190.7	46.0	0.008	0	0
n-C_{10}	617.6	21.1	0.49	0	0

Table 2: Critical properties for C_1/n-C_{10} mixture

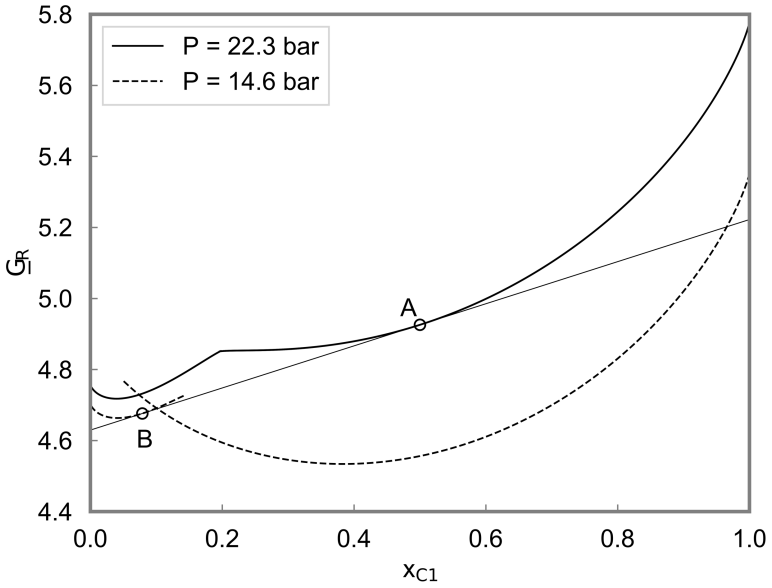

Figure 6: Gibbs free energy curves of equimolar C_1/n-C_{10} binary mixture at 560.9 K and 22.3 bar at equilibrium with 14.6 bar.

The distance between the tangent line and the Gibbs free energy in Figure 6 gives the tangent-plane distance (TPD) as shown in Figure 7. The correct solution of the phase stability problem for the reference fluid (Point A) is given by the incipient phase at Point B. However, Figure 7 shows a large segment of negative TPD values with the stationary point C. By observation of the two Gibbs free energy surfaces in the entire composition space, this stationary point C can be easily identified as a non-physical part of the Gibbs free energy for the oleic phase. Numerical algorithms for stability analysis must avoid converging to the stationary point in the non-physical part of the Gibbs free energy curve. One solution proposed by Neshat et al. (2019) is to initiate the stability test using the compositions at the stationary points of the TPD with no capillary pressure. When the trivial solution A is discarded, point D can be used to initialize a local minimization algorithm to converge to the correct solution of point B. This method partly solves the

paradox presented by Rezaveisi et al. (2018). However, it is not a fundamental solution to the problem as demonstrated in Section 3.2.3.

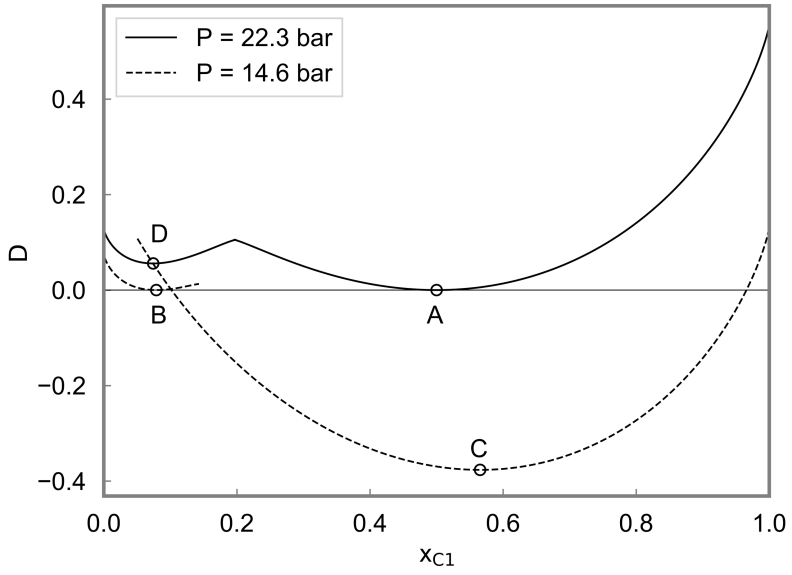

Figure 7: Gibbs free energy TPD curves for C_1/n-C_{10} mixtures at 560.9 K for a reference equimolar mixture A at 22.3 bar and an incipient phase composition B.

Another challenge of using the Gibbs free energy for stability analysis is that the conventional method for root selection of the cubic EOS is not robust when capillary pressure is considered. Neshat et al. (2018) showed that for some conditions the equilibrium root of the EOS may not be the lowest Gibbs free energy one. Figure 8 illustrates this phenomenon with the Gibbs free energy curves for an equimolar mixture of methane and n-butane at 333 K at 36.0 bar. Table 1 shows the critical properties for this mixture of methane and n-butane. The capillary pressure for the incipient phase is assumed to be 15.9 bar. At these conditions, there are two stable states for the equimolar mixture denoted S_1 and S_2 as shown in Figure 8, where S_1 and S_2 correspond to the single-phase and two-phase mixture solutions respectively. The liquid and vapor Gibbs free energy

curves are represented by the solid and dashed lines at 36 and 10.1 bar respectively in Figure 8. At compositions where the cubic EOS had more than one root, both the upper and lower roots are considered. We observe that the correct equilibrium solution is that of the two-phase state by comparing the total Gibbs free energy of S_1 and S_2. For the equilibrium liquid mixture composed of 18 mol% methane, the cubic EOS has three roots. The upper and lower roots are marked as roots A and B respectively on Figure 8. Despite being the highest Gibbs free energy root, root A is the correct one at equilibrium because the phase configuration AC represents the global minimum of the total Gibbs free energy of the equimolar mixture. Therefore, the root selection method is not reliable for computing thermodynamic state calculations with the Gibbs free energy.

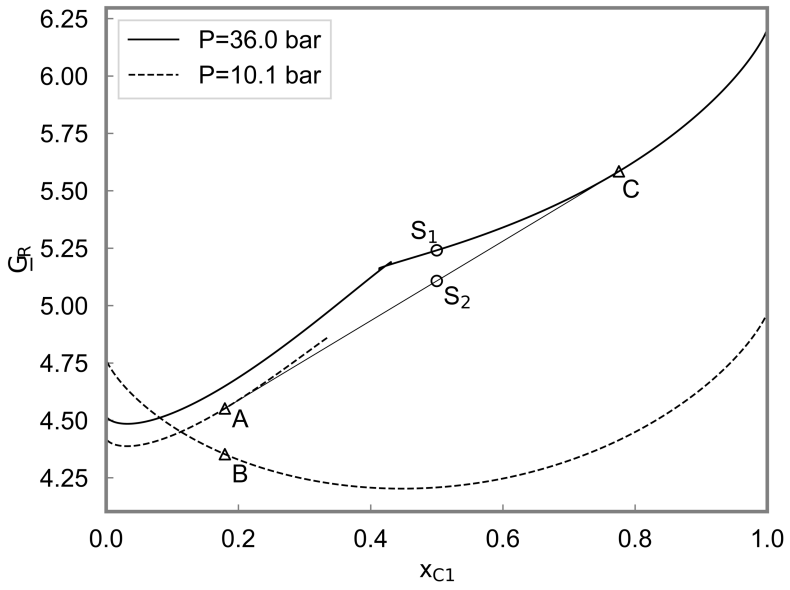

Figure 8: Gibbs free energy curves for equimolar mixture C_1/n-C_4 mixture at 333 K, 36 bar, and at capillary pressure of 25.9 bar

Though most of the literature published on equilibrium calculation uses the Young-Laplace capillary pressure model, saturation-based capillary pressure models are more accurate for predicting capillary pressure and phase behavior in tight reservoir rocks. Yan

et al. (2017) designed the first stability test for tight reservoirs using a saturation-based capillary pressure model. They show that it is necessary to couple the SS stability analysis at constant capillary pressure with phase-split calculations in order to obtain the necessary input parameters of saturation in the capillary pressure model. This coupling is executed in a sequential manner as follows.

Step 1. Initiate the capillary pressure at 0 or using the value in the previous time-step.

Step 2. Run the SS stability test with constant capillary pressure.

Step 3. If calculations converged, determine the stability based on the sign of the TPD at convergence.

Step 4. Run the SS phase-split calculation with constant capillary pressure.

Step 5. Evaluate the capillary pressure and return to step 2.

The convergence criterion used in step 3 was not clearly stated for this coupled phase-split/phase-stability analysis algorithm. Moreover, the authors did not address concerns over the potential failures of stability analysis algorithms using the TPD criterion for stability analysis. Neshat et al. (2019) presented an alternative coupled algorithm, though it was only designed for a mixture near the dew point. In Appendix A, we present a slightly modified general version of the algorithm presented by Neshat et al. (2019).

In the coupled phase-stability/-split calculations, the composition of the stationary point to the TPD is used to initiate the phase-split calculation (Neshat et al., 2019) even when the TPD is positive. The thermodynamic conditions for such stationary points with positive TPD are referred to as the "shadow-phase region" by Rasmussen et al. (2006). This region is located between the phase envelope boundary represented by a solid line and the dashed line in the single-phase region for an example phase envelope in Figure 9. Rasmussen et al. (2006) proposed a method to not perform phase stability analysis outside

of the shadow phase region during equation-of-state compositional flow simulation for computational efficiency. This represents an important contribution in the literature for computational efficiency and relies on the identification of the Gibbs free energy shadow-phase region. In Chapter 3, we prove the Gibbs free energy shadow-phase region is not relevant for stability analysis with capillary pressure and that the Helmholtz free energy one should be used instead.

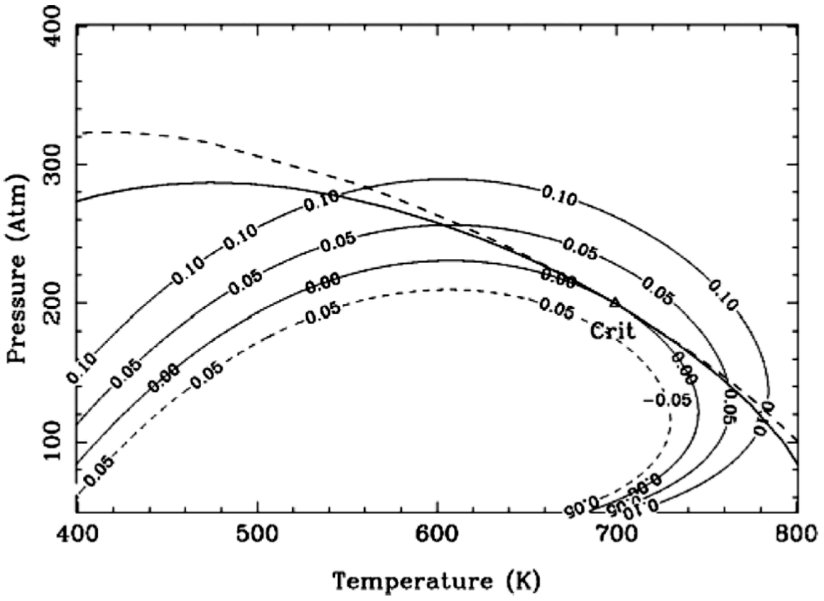

Figure 9: Shadow-phase region for hydrocarbon mixture on a pressure-temperature diagram (Rasmussen et al., 2006).

2.2.2 Stability Analysis With the Helmholtz Free Energy

A robust phase-stability analysis algorithm is essential for compositional reservoir simulation. However, the conventional methods using the Gibbs free energy offer several challenges, many of which have not been solved yet. The Helmholtz free energy is an alternative thermodynamic function which has also been used for stability analysis.

As opposed to the Gibbs free energy, there is no conventional algorithm for stability testing using the Helmholtz free energy. This is because equilibrium calculations using the

Helmholtz free energy have received far less attention in the literature than did the algorithms based on the Gibbs free energy. Nagarajan et al. (1991) implemented the first stability test based on the Helmholtz free energy, using component molar density as a variable although they did not discuss the details of their algorithm. They demonstrated that the Helmholtz free energy is globally smoother than Gibbs free energy which can have discontinuous first derivatives and concluded that the Helmholtz free energy-based equilibrium calculations are more convenient for gradient-based minimization methods such as Newton-Raphson.

Firoozabadi and Mikyska (2012) derived the SS stability analysis algorithm with the Helmholtz free energy using component molar density as the independent variables. They showed that the SS independent variable update equations can be derived by rearranging the stationarity condition in equation (2.39) as

$$d_i^{k+1} = d_{ir}\Psi_{ir}/\Psi_i^k, \text{ where } i = 1, \dots, N_c \tag{2.69}$$

where Ψ_i as a new thermodynamic function defined by $\Psi_i(\underline{\mathbf{d}}) = \underline{V}P\phi_i = f_i/d_i$ $(i = 1, \dots, N_c)$.

However, Firoozabadi and Mikyska (2012) reported that that SS algorithm was not robust because the iterates sometimes jumped out of the feasible region defined by the following condition:

$$\underline{V} > b_m \Leftrightarrow \sum_{i=1}^{N_c} d_i b_i > 1 \tag{2.70}$$

where b_m is the mixture co-volume parameter and b_i is the component specific co-volume parameter as defined in Section 2.1.3. Firoozabadi and Mikyska (2012) also claimed that they found some cases where the algorithm diverged from the correct solution no matter how close the initial guess was to the desired solution. Additionally, Firoozabadi and Mikyska (2012) claimed that unlike the Gibbs free energy SS, the SS algorithm converged to saddle point for many cases. No example cases were demonstrated to support their claim.

Firoozabadi and Mikyska (2012) provided more reasons for the lack of robustness of the SS algorithms which will not be discussed here due to a lack of support for their claims.

Instead of using SS, Firoozabadi and Mikyska (2012) recommended using Newton-Raphson based algorithms to compute the local minima of the TPD function. All the following publications followed the recommendation of Firoozabadi and Mikyska (2012) and improved the Newton-Raphson stability analysis by using various different minimization variable transformations on the component molar density.

Castier (2014) minimized the TPD using $\ln(\underline{\mathbf{d}})$ as the minimization variable. Nichita (2017) later minimized the TPD with a new independent variable $\boldsymbol{\delta} = 2\sqrt{\underline{\mathbf{d}}}$ based on an optimal scaling of the Hessian matrix to reduce its conditioning number. The Hessian matrix in terms of the component molar density $\underline{\mathbf{d}}$ is

$$\partial^2 \mathrm{D}/\,\partial \mathrm{d_i}\,\partial \mathrm{d_j} = \partial(\ln(\Psi_\mathrm{i}\mathrm{d_i}))/\,\partial \mathrm{d_j} = \partial(\ln(\Psi_\mathrm{i}))/\,\partial \mathrm{d_j} + \delta_{\mathrm{ij}}/\mathrm{d_i}\,, \tag{2.71}$$

where $\mathrm{i} = 1, \ldots, \mathrm{N_c}$, and $\mathrm{j} = 1, \ldots, \mathrm{N_c}$, and δ_{ij} is the Kronecker delta such that $\delta_{\mathrm{ij}} = 1$ if $\mathrm{i} = \mathrm{j}$, otherwise $\delta_{\mathrm{ij}} = 0$. According to Nichita (2017), the diagonal matrix $\mathbf{U}$ containing the elements $\delta_{\mathrm{ij}}/\mathrm{d_i}$ which may span several orders of magnitude especially for mixtures with trace elements certain components. This causes the Hessian matrix to often be ill-conditioned, and the Newton-Raphson methods become significantly slower especially near singularities. The solution to improving the conditioning of the Hessian matrix is then to find a transformation variable $\boldsymbol{\delta}(\underline{\mathbf{d}})$ such that $\mathbf{U}$ becomes equal to the identity matrix. This can be accomplished by solving the following equation.

$$(1/\mathrm{d_i})(\partial \mathrm{d_i}/\,\partial \delta_\mathrm{i})(\partial \mathrm{d_j}/\,\partial \delta_\mathrm{j}) = 1, \text{ where } \mathrm{i} = \mathrm{j} = 1, \ldots, \mathrm{N_c} \tag{2.72}$$

One transformation variable which solves equation (2.72) is $\boldsymbol{\delta} = 2\sqrt{\underline{\mathbf{d}}}$. Nichita (2017) then showed that the condition number for the Hessian matrix calculated with independent variable $\boldsymbol{\delta}$ is consistently lower than that calculated with $\underline{\mathbf{d}}$ and $\ln(\underline{\mathbf{d}})$. Additionally, the number of iterations for the optimal scaling variable $\boldsymbol{\delta}$ is also consistently

lower than it is for the other two variables. Nichita (2018) then compared the performance of the TPD minimization algorithm with **δ** against Newton-Raphson algorithms using other independent variables such as the component molar density **d**, number of moles **N** and total volume V, and a combination of conventional Gibbs free energy SS and Newton-Raphson. His results show that the algorithm which converged within the least number of iterations was the stability analysis using Gibbs free energy with a combination of SS and Newton-Raphson. Among the stability analysis methods using the Helmholtz free energy, the most performant was the optimal scaling variable **δ**.

The conventional method to compute the initial guesses for the Gibbs free energy stability analysis cannot be used to initialize the Helmholtz free energy stability tests because the pressure of bulk phase computed by the EOS may be negative and therefore incompatible with Raoult's law for computing K-values based on Wilson's correlation. Nichita et al. (2006; 2009) used some arbitrary low pressure when the bulk pressure was negative. However, this initial guess was often observed to not converge to the correct solution. That is why, they used a stochastic tunneling method to search for other possible local minima after convergence. Castier (2014) initialized the stability test by evaluating the TPD at 5000 discrete points in **d** variable space then initialized a Newton-Raphson minimization method at the local minima of the discrete points. After convergence, he used a stochastic tunneling method to look for other local minima and ensure convergence to the global minimum. Both these methods are very computationally expensive and therefore not useful for reservoir simulators. A more efficient method was proposed by Firoozabadi and Mikyska (2012) and Nichita (2017), then used in many algorithms (Jindrova and Mikyska, 2013; Jindrova and Mikyska, 2015; Nichita, 2017; Nichita, 2018; Nichita, 2019a). It uses Wilson's correlation for vapor pressures to evaluate the approximate composition and pressure of the incipient phase based on Raoult's law. The bubble point pressure can

then be analytically estimated as the weighted arithmetic average of the vapor pressures of each component in the mixture

$$P^{bbl} = \sum_{i=1}^{N_c} z_i P_i^{vap}. \tag{2.73}$$

The vapor-like incipient phase composition can then be estimated using Raoult's law as

$$x_{iV} = P_i^{vap}/P^{bbl}. \tag{2.74}$$

Then, the dew point pressure can also be analytically estimated as the weighted geometric average of the vapor pressures of each component in the mixture

$$P^{dew} = 1/(\sum_{i=1}^{N_c} z_i/P_i^{vap}). \tag{2.75}$$

The liquid-like incipient phase composition can be estimated using Raoult's law as

$$x_{iL} = P_i^{vap}/P^{dew}. \tag{2.76}$$

The molar volume for both initial guesses can be computed by solving the cubic EOS of the initial guess trial phase compositions. Firoozabadi and Mikyska (2012) suggest using both stable roots of the cubic EOS solution if available as separate initial guesses to increase the chances of converging to the global minimum.

Kou and Sun (2018) derived a stability criterion for mixtures in tight rocks based on the Helmholtz free energy. The expression for the TPD that they derive differs from the Helmholtz free energy by the term γP_{cap} as follows:

$$D(\underline{\mathbf{d}}) = \sum_{i=1}^{N_c} d_i(\ln(f_i) - \ln(f_{ir})) - (P - P^r - \gamma P_{cap})/RT \geq 0 \tag{2.77}$$

where γ is equal to 1 when the trial phase is gas and is equal to -1 otherwise. Kou and Sun (2018) then used a dynamic model to compute the minimum of equation (2.77). The stationarity condition is fulfilled when the gradient of the TPD is equal to 0. Kou and Sun (2018) derive the stationarity condition for the Helmholtz free energy TPD of fluid mixture as

$$\ln(f_i) - \ln(f_{ir}) + (\gamma/RT)\,\partial P_{cap}/\partial d_i = 0, \text{ where } i = 1, \dots, N_c. \tag{2.78}$$

They evaluate the derivative of the Young-Laplace capillary pressure as a function of the component molar density of the trial phase for a fixed reference phase density.

$$\partial P_{cap} / \partial d_i = (2\cos(\theta)/\mathcal{R}) \, \partial\sigma / \partial d_i, \text{ where } i = 1, \dots, N_c. \quad (2.79)$$

where θ is the contact angle, $\mathcal{R}$ is the average pore radius, and σ is the IFT between the oil and the gas phase calculated with the parachor model as explained in Section 2.1.4.1. However, they do not explain or analyze the difference between phase equilibrium calculations based on the Helmholtz and Gibbs free energy.

Nichita (2019a) used stability criterion (2.77) to derive a stability analysis algorithm using the Newton-Raphson method with the independent variable $\boldsymbol{\delta}$. The gradient of the TPD is evaluated to be the same as that of Kou and Sun (2018), and the Hessian of the TPD includes a capillary pressure term.

$$H_{ij} = \partial \ln(f_i) / \partial d_j + (\gamma/RT) \, \partial P_{cap} / \partial d_i \, \partial d_j = 0, \quad (2.80)$$

where $i = 1, \dots, N_c$ and $j = 1, \dots, N_c$.

Nichita (2019a) claimed that the advantage of using the Helmholtz free energy instead of Gibbs free energy for stability analysis in tight reservoirs is that correlations for capillary pressure tend to be explicit in volume, which simplifies the expression for its derivatives. This observation about the advantage of volume-based methods for calculations involving capillary pressure was also supported by Sandoval et al. (2019). Chapter 3 analyzes in more depth the fundamental differences and advantages to using the Helmholtz free energy for phase-stability testing.

The algorithms of Kou and Sun (2018) and Nichita (2019a) predict an erroneous phase envelope boundary which does not match that predicted by Gibbs free energy-based algorithms. Nichita (2019a) illustrated this mismatch by comparing the phase envelope boundary of a hydrocarbon fluid mixture predicted by his method with the one predicted by the algorithm of Sherafati and Jessen (2017) which is based on Gibbs free energy. The

dew point curves for an oil mixture in a 10-nm capillary tube predicted by the two algorithms are shown in Figure 10.

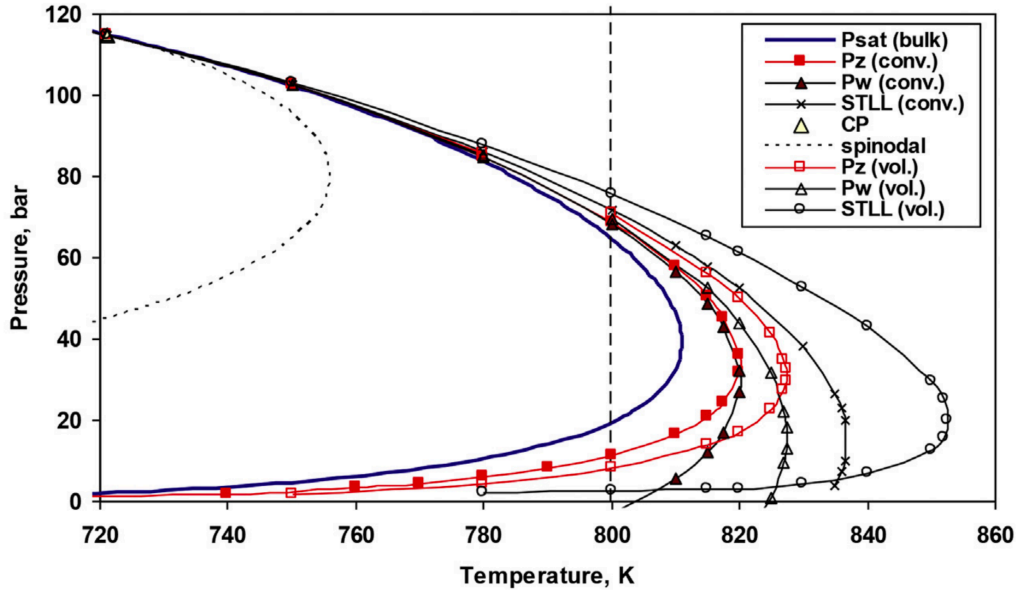

Figure 10: Phase pressures at the dew point for hydrocarbon mixture in a capillary tube of 10 nm predicted by Nichita's Helmholtz free energy-based algorithm (2019) denoted as "vol." and the Sherafati and Jessen's algorithm (2017) denoted as "conv.".

Nichita (2019b) later admitted that this mismatch was caused by the presence of the capillary pressure term in the stationarity condition of equation (2.78). At equilibrium, the fugacity of the reference and trial phases are equal, however the capillary pressure derivative is not equal to 0. Therefore, the stationarity condition for the TPD is not fulfilled on the phase envelope boundaries. This indicates that the phase-stability test formulated by Kou and Sun (2018) and Nichita (2019a) is incorrect. Chapter 3 presents the correct formulation and algorithms for phase-stability testing for tight porous media using the Helmholtz free energy.

CHAPTER 3: Stability Analysis Using the Helmholtz Free Energy for Tight Porous Media

Flash calculations in reservoir simulators typically use stability analysis to determine the number of phases at equilibrium. Accurate simulation of multi-phase equilibrium in tight reservoirs requires the inclusion of the effect of capillary pressure on the phase behavior. Most studies which attempt to include the effect of capillary pressure in stability analysis use methods based on the Gibbs free energy. These methods are not robust because the Gibbs free energy curve depends on the pressure of the incipient phase. This gives the motivation for using the Helmholtz free energy instead since it is a function of volume instead of pressure. However, published stability analysis methods for tight reservoirs were ill-formulated. Moreover, the advantages of using the Helmholtz free energy for numerical stability analysis instead of the Gibbs free energy are not clear. In this chapter, we present correct the formulation of the stability analysis using the Helmholtz free energy and use concrete examples to illustrate the advantages of using the Helmholtz free energy for stability analysis.

3.1 Formulation and Algorithm

In this section, we present the correct formulation for the stability analysis for phase equilibrium in the presence of a curved interface and a general approach for its implementation in a numerical stand-alone algorithm.

3.1.1 Formulation

The first and second laws of thermodynamics require that the Helmholtz free energy of the system be minimized at an equilibrium state at a specified total molar volume, temperature, and overall composition subject to material balance. With these thermodynamic specifications, a phase is said to be stable if any possible perturbation

cannot lower the total Helmholtz free energy of the system. That is, the phase of interest ("reference phase") is stable if

$$dA_{\text{total}} = dA_{\text{r}} + dA_{\sigma} + dA \tag{3.1}$$

is non-negative for any possible incipient phase. In Equation (3.1), dA_{T}, dA_{r}, dA_{σ}, and dA respectively represent the change in the Helmholtz free energy for the total system, the reference phase, the interface, and the incipient phase. The change in the Helmholtz free energy is

$$dA = -SdT - PdV + \sum_{i=1}^{N_C} \overline{G}_i dN_i \tag{3.2}$$

for the incipient phase,

$$dA_{\text{r}} = -S_{\text{r}}dT_{\text{r}} - P_{\text{r}}dV_{\text{r}} + \sum_{i=1}^{N_C} \overline{G}_{ir} dN_{ir} \tag{3.3}$$

for the reference phase, and

$$dA_{\sigma} = -S_{\sigma}dT_{\sigma} - P_{\sigma}dV_{\sigma} + \sum_{i=1}^{N_C} \overline{G}_{i\sigma} dN_{i\sigma} + \sigma da \tag{3.4}$$

for the interface.

The stability analysis is subject to the material balance, the volume balance, and constant temperature as follows:

$$dN_{ir} + dN_{i\sigma} + dN_i = 0 \tag{3.5}$$

$$dV_{\text{r}} + dV_{\sigma} + dV_i = 0 \tag{3.6}$$

$$dT_{\text{r}} = dT_{\sigma} = dT = 0. \tag{3.7}$$

With these constraints, dA_{T} is written as

$$\begin{aligned} dA_{\text{total}} = &-(P - P_{\text{r}})dV - (P_{\sigma} - P_{\text{r}})dV_{\sigma} + \sum_{i=1}^{N_C}\left(\overline{G}_i - \overline{G}_{ir}\right)dN_i \\ &+ \sum_{i=1}^{N_C}\left(\overline{G}_{i\sigma} - \overline{G}_{ir}\right)dN_{i\sigma} + \sigma da. \end{aligned} \tag{3.8}$$

Supposing that the second and fourth terms are negligible in comparison to the other terms on the right-hand side of Equation (3.8), dA_{T} is approximated as

$$dA_{\text{total}} = -(P - P_{\text{r}})dV + \sum_{i=1}^{N_C}\left(\overline{G}_i - \overline{G}_{ir}\right)dN_i + \sigma da. \tag{3.9}$$

With no loss of generality, dA_{total} is divided by $RTdV$, which is a positive real number within this stability analysis. Then, the determinant for the phase stability problem is

$$D = d(A_{total}/RT)/dV = \left[\sum_{i=1}^{N_c}(\overline{G}_i - \overline{G}_{ir})d_i - (P - P_r) + P_*\right]/RT, \quad (3.10)$$

where $d_i = dN_i/dV = x_i/\underline{V}$ $(i = 1, \ldots, N_c)$ as used in (Nagarajan, 1991). Note that $\underline{V} = 1/\sum_{i=1}^{N_c} d_i$. P_* physically represents $\sigma da/dV$, which depends on the phase properties and force balances with the local interfacial geometries. The D function spans the $\mathbf{d}$ space, and can be considered as the distance between the A/RTV function and the plane that is parallel to the tangent plane to the A/RTV function defined at $\mathbf{d}_r$ (see Section 3.2 for more details of the function).

The fundamental procedure for the phase stability analysis is to find stationary points of D in $\mathbf{d}$ space of N_c dimensions, and check the sign of D at the identified stationary points for a given T, $\underline{V}_T$, and the overall (or reference-phase) composition $\mathbf{x}_r$. If D is found to be negative at any $\mathbf{d}$, the reference phase is determined to be unstable.

The stationarity conditions for D in $\mathbf{d}$ space are derived as

$$F_i = \partial D/\partial d_i = \ln(f_i) - \ln(f_{ir}) = 0, \text{ where } i = 1, \ldots, N_c \quad (3.11)$$

for which the Gibbs-Duhem equation (2.7) is used. In the above equation, f_i is the fugacity of component i. Note that P_* is a scalar value or function to be specified; e.g., the Young-Laplace and saturation-based models relate P_* to properties of the equilibrium phases that satisfies $F_i = 0$ and the associated constraints for all i. Hence, the derivative of the P_* term is rigorously zero for the stationarity conditions.

According to the second law of thermodynamics, mixtures with non-positive-definite Helmholtz Hessian are intrinsically unstable. Therefore the P_* term is undefined when the Helmholtz free energy Hessian of the reference phase and the stationary point is not positive definite. Therefore, the stability analysis should be bypassed when the

reference phase Helmholtz Hessian is not positive definite as it is intrinsically unstable. Otherwise, the correct method to avoid the non-positive definite solutions to equations (3.11) is to compute the global minimum of the D function. The D function at a stationary point (D_{SP}) is

$$D_{SP} = (P_r - P + P_*)/RT. \tag{3.12}$$

If $D_{SP} < 0$, $dA_{total} < 0$ at the stationary point identified, noting that $dV > 0$; therefore, the reference phase is determined to be unstable. If $D_{SP} = 0$ at $\mathbf{d}$ with $\mathbf{x} \neq \mathbf{x_r}$, $P_* = P - P_r$, which is the differential pressure between the incipient and reference phases at a phase boundary. In general cases, however, P_* is not directly related to capillary pressure within this research except for phase boundary calculations, in which the incipient and reference phases are at equilibrium.

In summary, the phase stability analysis for tight porous media using the Helmholtz free energy is formulated as

find $\mathbf{d}_{sp} \in \mathbb{R}^{N_c}$ such that $\mathbf{F} = 0$ and $\nabla\mathbf{F}$ is positive-definite, then check if $D_{SP} < 0$,

given $\mathbf{F} \in \mathbb{R}^{N_c}$ at T, $\underline{V}$, and $\mathbf{x_r}$ with a specified value or function for P_*.

This analysis is usually repeated using multiple initial guesses because it is generally difficult to ensure that the global minimum of D is located in $\mathbf{d}$ space using a cubic equation of state. The search for stationary points is a series of local minimization of D in $\mathbf{d}$ space because the Jacobian matrix of $\mathbf{F}$ is the Hessian matrix of D.

3.1.2 Algorithm

As in Nichita (2017), the independent variables for minimizing D are $\delta_i = 2\sqrt{d_i}$ such that $i = 1, \ldots, N_c$. A stationary point of D in $\boldsymbol{\delta}$ space is located by local minimization with linear constraints $\sum_{i=1}^{N_c} b_i x_i < \underline{V}$, where b_i is the co-volume parameter of component i. That is,

minimize $D(\boldsymbol{\delta})$

subject to $\mathbf{b} \cdot \mathbf{d} < 1$.

A step-wise description of the algorithm for each local minimization is given below. This algorithm is usually repeated for different initial guesses as discussed previously.

Step 1. Calculate the Hessian of D and determine its positive definiteness at the reference phase composition, $\mathbf{x}_r$. If it is positive definite, go to Step 2. Otherwise, the reference phase is unstable, and stop.

Step 2. Initialization of $\mathbf{d}$

2.1 Initialize the incipient phase **x** and P using the method of user's choice.

2.2 Solve the equation of state for molar volume of the incipient phase V.

2.3 Compute the initial $\mathbf{d}$ and the iteration variables $\boldsymbol{\delta}$. Set the iteration index k = 0. $\boldsymbol{\delta}^k = \boldsymbol{\delta}$.

Step 3. Minimization of D using $\boldsymbol{\delta}$

3.1 Compute the gradient of D at $\boldsymbol{\delta}^k$. This gradient is denoted as $\mathbf{g}^k$.

3.2 Compute the Hessian matrix of D at $\boldsymbol{\delta}^k$. This matrix is denoted as $\mathbf{H}^k$.

3.3 Solve for the Newton direction $\Delta\boldsymbol{\delta}^k$ through the modified Cholesky decomposition. $\mathbf{H}^k$ is modified if it is weakly positive definite or non-positive definite.

$$\mathbf{H}^k \Delta\boldsymbol{\delta}^k = -\mathbf{g}^k$$

3.4 Use the line-search technique to optimize the step-size (Nichita, 2017) and confirm the feasibility of the iterate: $\mathbf{b} \cdot \mathbf{d} < 1.0$. If unfeasible, reduce the step size λ until $\boldsymbol{\delta}^{k+1}$ becomes feasible.

$$\boldsymbol{\delta}^{k+1} = \boldsymbol{\delta}^k + \lambda\Delta\boldsymbol{\delta}^k$$

$k \leftarrow k + 1$

3.5 Compute $\mathbf{d}^k$, $\underline{V} = 1/\sum_{i=1}^{N_c} d_i$, P, and $\mathbf{x}^k = \underline{V}\mathbf{d}^k$. Then, calculate the residual $r^k = \left\|\mathbf{g}^k\right\|_\infty$. If $r^k < \varepsilon_{sp}$, continue to Step 4. Otherwise, go to Step 3.2.

Step 4. Check the proximity of $\mathbf{x}$ to $\mathbf{x}_r$. If $\|\mathbf{x} - \mathbf{x}_r\|_\infty > \varepsilon_{ts}$, $\mathbf{x}$ is considered as a non-trivial stationary point and continue to Step 5. Otherwise, stop.

Step 5. Calculate D_{sp} at $\mathbf{x}$. If $D_{sp} < 0$, the reference phase $\mathbf{x}_r$ is unstable.

If all tested initial guesses do not find the reference phase to be unstable, it is assumed to be stable. Remarks for some steps are given here. In Step 2.1, a common choice is to use Raoult's law along with a certain vapor-pressure correlation (e.g., Wilson's correlation) for either vapor-like or liquid-like phase; however, other initialization methods have been also proposed (Nagajaran, 1991; Nichita et al., 2006; Castier, 2014). In Step 2.2, if there are two real roots, both roots can be tested as presented in (Firoozabadi and Mikyska, 2012). In Step 3.5, the equation of state is used to explicitly compute P by using $\underline{V}$. In Step 5, P_* is specified as a scalar quantity or function. Common choices for such a function are the Young-Laplace and saturation-based models. In this research, ε_{sp} and ε_{ts} are 10^{-9} and 10^{-7}, respectively.

3.2 CASE STUDIES

The main objective of this section is to demonstrate the main advantages of using the Helmholtz free energy over the conventional method using the Gibbs free energy for phase stability analysis with a curved interface. The thermodynamic model used is the Peng-Robinson equation of state with the van der Waals mixing rules. Volume shift is not used within this research as it affects the fugacity equations when equilibrium phases have different pressures (Kumar and Okuno 2015). The conventional method compared with the new method here is based on Neshat et al. (2019) with slight modifications.

3.2.1 Case 1

The main objective of Case 1 is to clarify the differences between this report and other publications on phase stability analysis with capillary pressure (Kou and Sun 2018, Nichita 2019ab). Kou and Sun (2018) presented their derivation of the phase stability criterion using the Helmholtz free energy in the presence of capillary pressure, which is quite different from that in this study (Section 3.1.1).

The important consequence of the differences lies in the P_* term. To obtain the result of Kou and Sun (2018), this term must be replaced by γP_{cap} , where $\gamma = 1$ for a gas phase and $\gamma = -1$ for a liquid phase. Then, their stationarity criterion contained the derivative of γP_{cap} with respect to their independent variables, which are the component mole numbers in the incipient phase. Kou and Sun's derivation resulted in the statement of Nichita (2019b) that $F_i = 0$ is not the stationarity condition of the D function in $\mathbf{d}$ space.

As described previously, P_* is $\sigma da/dV$ and use of it as differential pressure between two phases necessitates that $dA_{total} = 0$ and, therefore, $F_i = 0$ for $i = 1, \ldots, N_c$. That is, only if the stationarity conditions (i.e., fugacity equations) are satisfied, P_* can be specified by using a capillary-pressure model, for example, by the Young-Laplace or saturation-based model. Otherwise, P_* must be a numerical value to be specified prior to the computation. In either case, the derivative of the P_* term must be zero for the stationarity conditions of D.

The γP_{cap} term remained in their stationarity conditions in Kou and Sun (2018) and Nichita (2019). Therefore, the component fugacities are not equal between the reference phase and a stationary point found by their methods, as confirmed in this research. This is likely the reason why calculation results were inconsistent between Nichita's method using the Helmholtz free energy and the conventional method using the Gibbs free energy. Nichita (2019a) showed that the dew point curve by his method based on the Helmholtz

free energy deviated from the one from the conventional method using the Gibbs free energy for the fluid "SJ15" taken from Sherafati and Jessen (2017). However, the results for a given thermodynamic problem must be identical whether the problem is formulated by minimization of the Helmholtz free energy or the Gibbs free energy.

The new method developed in this research is used to calculate dew point curves for the fluid "SJ15" with no curved interface and with a capillary radius of 10 nm for the Young-Laplace model. Table 3 shows the fluid properties for SJ15. As in their papers, a parachor exponent of 4 is used. Unlike in Sherafati and Jessen (2017) and Nichita (2019), the Peng-Robinson equation of state is used with no volume shift here, but it is used for both approaches using the Gibbs and Helmholtz free energy for a fair comparison. A detailed description for the Gibbs free energy algorithm used in this study is described in Appendix A.

Figure 11 shows the calculated dew point curves using the new method and the conventional method using the Gibbs free energy. The capillary tube's surface is assumed to be liquid-wet; therefore, capillary pressure causes the two-phase region to expand in this diagram. The dew-point curve without capillary pressure is given by the solid line. The dew-point curve for the 10-nm tube is shown by the bold dashed line for the conventional method and by hollow circles for the new method using the Helmholtz free energy. The figure also shows the oil-phase pressures for the phase boundary conditions for the 10-nm tube. As expected, the new and conventional methods give identical results, confirming the consistency between the Helmholtz and Gibbs formulations.

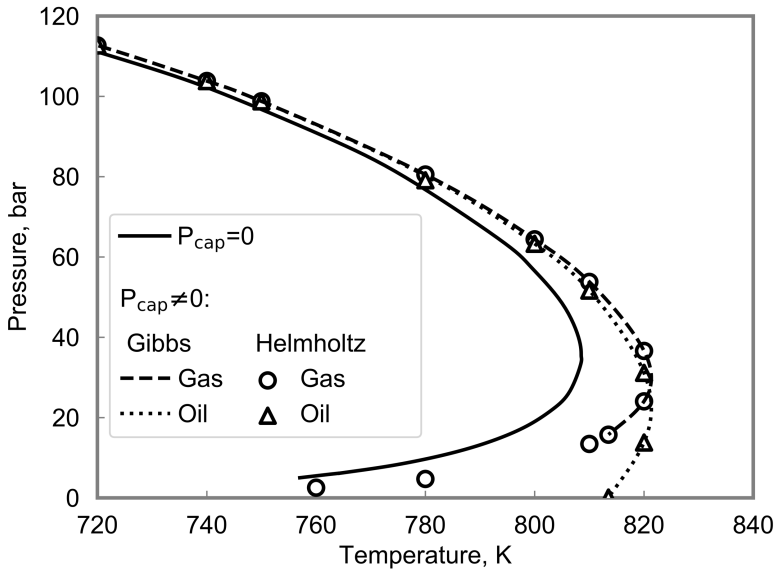

Figure 11: Phase pressures at the dew point for SJ15 mixture at 0 capillary pressure and including capillary pressure using the algorithm based on the Gibbs free energy (as described in Appendix A) and the new algorithm using the Helmholtz free energy.

	Composition (mol fraction)	T_c (K)	P_c (bar)	ω	Π	BIP* N_2	CO_2	C_1
N_2	0.0018	126.2	34.045	0.04	43.85	0		
CO_2	0.0082	304.2	73.866	0.228	82.24	0.017	0	
C_1	0.2292	190.6	46.002	0.008	71.52	0.0311	0.12	0
C_2	0.0721	305.4	48.839	0.098	113.71	0.0515	0.12	0
C_3	0.0737	369.8	42.455	0.152	151.14	0.0852	0.12	0
i-C_4	0.0158	408.1	36.477	0.176	181.78	0.1033	0.12	0
n-C_4	0.0523	425.2	37.997	0.193	191.03	0.08	0.12	0
i-C_5	0.0225	460.4	33.843	0.227	224.14	0.0922	0.12	0
n-C_5	0.036	469.6	33.741	0.251	231.73	0.1	0.12	0
C_6	0.0484	507.4	29.688	0.296	274.03	0.08	0.12	0
PS1	0.196107	565.85	29.708	0.34612	331.01	0.08	0.1	0.028349
PS2	0.113893	683.44	20.103	0.57838	546.37	0.08	0.1	0.044813
PS3	0.066598	798.99	13.324	0.90175	884.73	0.08	0.1	0.062256
PS4	0.041047	899.68	9.697	1.19183	1391.97	0.08	0.1	0.077679
PS5	0.022355	1013.31	7.670	1.39383	2497.41	0.08	0.1	0.0952

Table 3: Fluid properties for SJ15 oil (Sherafati and Jessen, 2017)

*All others are 0.0

3.2.2 Case 2

Unlike the conventional methods using the Gibbs free energy, the new method involves only a single Helmholtz free energy surface, which improves the robustness especially for small pores (i.e., high capillary pressure). The conventional methods involve two Gibbs free energy surfaces for phase stability analysis: one fixed energy surface for the reference phase and another iterative energy surface for the incipient phase. Since the capillary pressure has to be part of the iterative solution, the conventional methods tend to fail when they attempt to minimize the total Gibbs free energy using two Gibbs surfaces with a large capillary pressure. This case study presents an example to demonstrate the advantage of using the Helmholtz free energy over the Gibbs free energy.

Table 2 shows the fluid properties for the equimolar mixture of methane and n-decane. Figure 12 shows the P-T diagram with no capillary pressure for this mixture, in which the condition for this case study is marked. The temperature is 560.9 K and the reference pressure is 22.3 bar. This is the equilibrium condition which was analyzed in Chapter 2 with the Gibbs free energy and TPD curves for the liquid and vapor phases in Figures 6 and 7. In Figure 7, Point C was identified as the stationary point of the TPD to a non-physical section of the Gibbs free energy. However, it is challenging for a computational algorithm to robustly and efficiently exclude such non-physical parts of the Gibbs free energy surfaces in composition space for general multicomponent mixtures. The fundamental cause of this issue is that the Gibbs free energy in composition space requires a pressure to be specified.

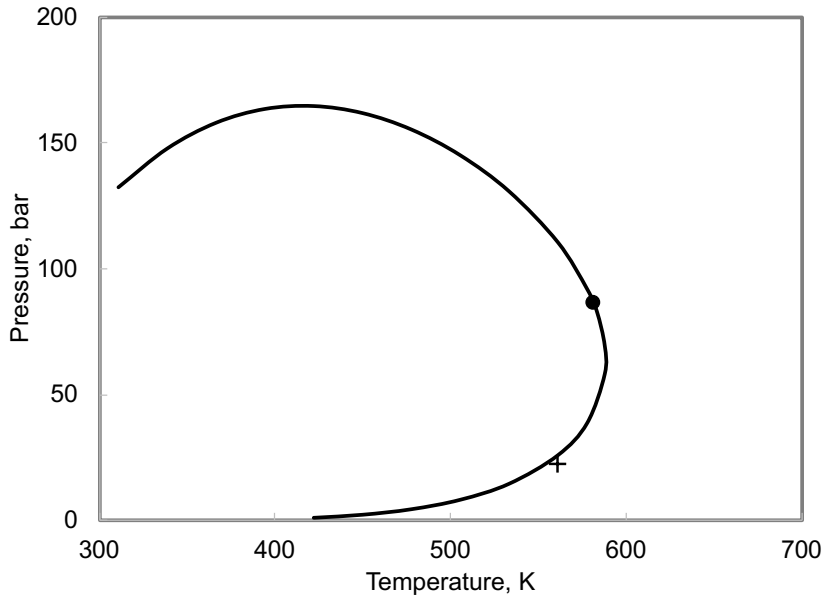

Figure 12: Phase envelope for equimolar methane/n-decane mixture on a P-T diagram. The "plus" sign indicates the conditions used for the stability analysis in case 2.

Figure 13a shows the Helmholtz free energy (A/VRT) in **d** space for the binary mixture (Table 1) at 560.9 K. The vertical axis has a unit of molar density, mol/L. The labels d_{C1} and d_{C10} represent the component molar densities of methane and n-decane, respectively, with the unit of mol/L. The non-linearity of the A/VRT surface is not obvious in Figure 13b, but it is clearly shown that only one function spans the **d** space.

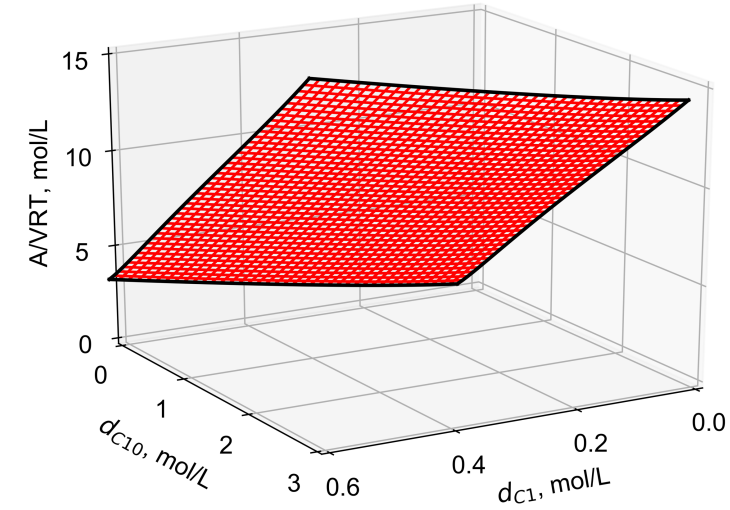

(a)

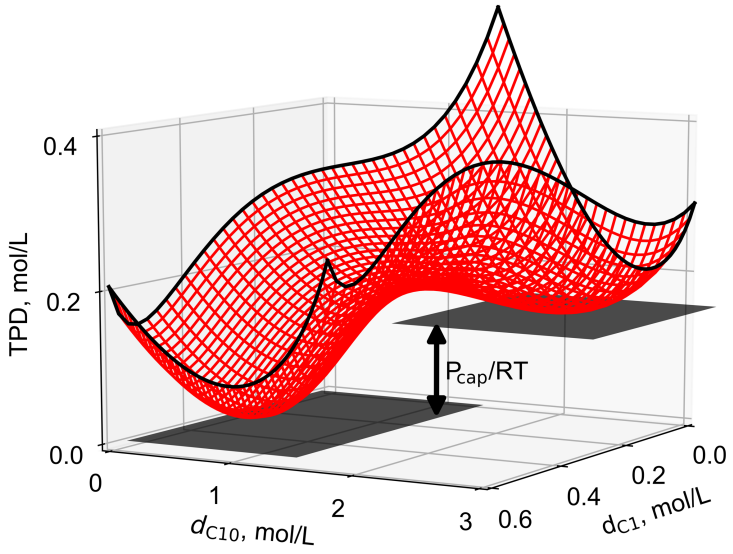

(b)

Figure 13: A/RTV surface (a) and TPD (b) for an equimolar mixture of methane and n-decane at 560.9 K and 1.176 L/mol.

More details of the Helmholtz free energy function in **d** space are described because it is important to have a graphical understanding of the function. It is straightforward to derive the expression for the tangent plane onto the A/VRT surface defined at the reference phase by repeating the derivation given in Section 3.1.1 with $dA_\sigma = 0$. The result corresponds to the determinant for phase stability analysis with no curved interface using the Helmholtz free energy, which is the tangent-plane-distance function as given as

$$D_T = \left[\sum_{i=1}^{N_C}\left(\overline{G}_i - \overline{G}_{ir}\right)d_i - (P - P_r)\right]/RT. \tag{3.13}$$

Figure 13b shows the D_T function for this case. The reference phase is given by (d_{C1}, d_{C10}) = (0.284, 0.284) and the incipient phase is (d_{C1}, d_{C10}) = (0.226, 2.65). Comparing equations (3.10) and (3.14) indicates that $P_*/RT = D - D_T$ at the incipient phase, which is 0.165 mol/L in this case.

3.2.3 Case 3

This section shows that the new method solves two types of inherent difficulties with the conventional methods using the Gibbs free energy. The example used is based on the equimolar mixture of methane and an Eagle Ford oil (Orangi et al., 2011), denoted here EF. Phase envelope boundaries shown in Figure 14 (no volume shift is used) are calculated by using the new method with no capillary pressure and with the saturation-based capillary pressure. The parameters used for the calculations are given in Table 4. Regions I and II represent the conditions for non-convergence with the conventional methods as described below.

γ	S_w	ϕ	k (μD)	b_o	b_g	a_o	a_g	S_{omin}	S_{gmin}
3.88	0	0.07	4.0	0.386	-0.193	1.0	0.06	0.06	0.06

Table 4: Capillary pressure parameters for Eagle Ford sample 2 from Neshat et al. (2018)

	Composition (mol fraction)	P_c (bar)	T_c (K)	ω	Π
N_2	0.000365	33.9349143	126.2	0.04	41
CO_2	0.006410	73.8431786	304.222222	0.225	78
C_1	0.656155	46.3944429	190.7	0.013	77.3
C_2	0.021570	48.8255536	305.427778	0.097	108.9
C_3	0.020740	42.5551214	369.888889	0.152	151.9
i-C_4	0.006750	36.46735	408.111111	0.185	181.5
n-C_4	0.016910	37.9562071	425.222222	0.201	191.7
i-C_5	0.009025	33.3269643	460.388889	0.2223	225
n-C_5	0.010705	33.7419143	469.783333	0.2539	233.9
n-C_6	0.023115	30.3078929	507.888889	0.3007	271
C_{7-10}	0.081485	27.7644286	589.166667	0.3739	311
C_{11-14}	0.060020	21.2093214	679.777778	0.526	471
C_{15-19}	0.050220	16.6393571	760.222222	0.6979	556.3
C_{20+}	0.036530	10.4151071	896.777778	1.0456	836.4

Table 5: Peng-Robinson EOS fluid model for equimolar mixture of Eagle Ford light oil and methane (Orangi et al., 2011)

BIP	N_2	CO_2	C_1	C_2	C_3	i-C_4	n-C_4	i-C_5	n-C_5
N_2	0								
CO_2	-0.02	0							
C_1	0.036	0.1	0						
C_2	0.05	0.135	0	0					
C_3	0.08	0.135	0	0	0				
i-C_4	0.095	0.13	0	0	0	0			
n-C_4	0.09	0.13	0	0	0	0	0		
i-C_5	0.095	0.125	0	0	0	0	0	0	
n-C_5	0.1	0.125	0	0	0	0	0	0	0
n-C_6	0.1	0.125	0	0	0	0	0	0	0
C_{7-10}	0.151	0.111	0.025	0.02	0.015	0.111	0.005	0.005	0.005
C_{11-14}	0.197	0.097	0.049	0.039	0.029	0.097	0.01	0.01	0.01
C_{15-19}	0.235	0.085	0.068	0.054	0.041	0.085	0.014	0.014	0.014
C_{20+}	0.288	0.07	0.094	0.075	0.056	0.07	0.019	0.019	0.019

Table 6: Non-zero entries in lower triangular BIP matrix for Eagle ford light oil mixture (Orangi et al., 2011)

3.2.3.1 Region I

In Region I, the conventional method results in non-convergence because of the overshoot of the iterative capillary pressure. This example is presented for the mixture (Tables 6 and 7) at 561 K and the reference phase pressure of 34.5 bar. The new method converges rapidly as shown in Figure 15 with $D_{SP} = -6.65$ mol/L < 0 indicating that the reference phase is unstable. The conventional method using the Gibbs free energy results in non-convergence when it attempts to solve the equation of state for the liquid phase at -76.7 bar. This pressure is lower than the minimum pressure on the pressure-volume isotherm for the liquid composition as shown in Figure 16.

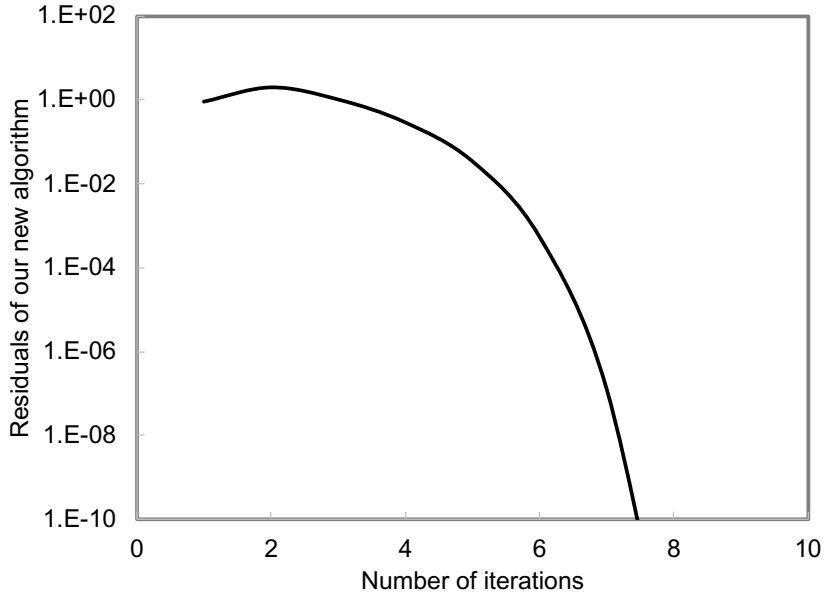

Figure 14: Quadratic convergence behavior for new stability analysis algorithm with an equimolar mixture of eagle ford light oil and methane in region I.

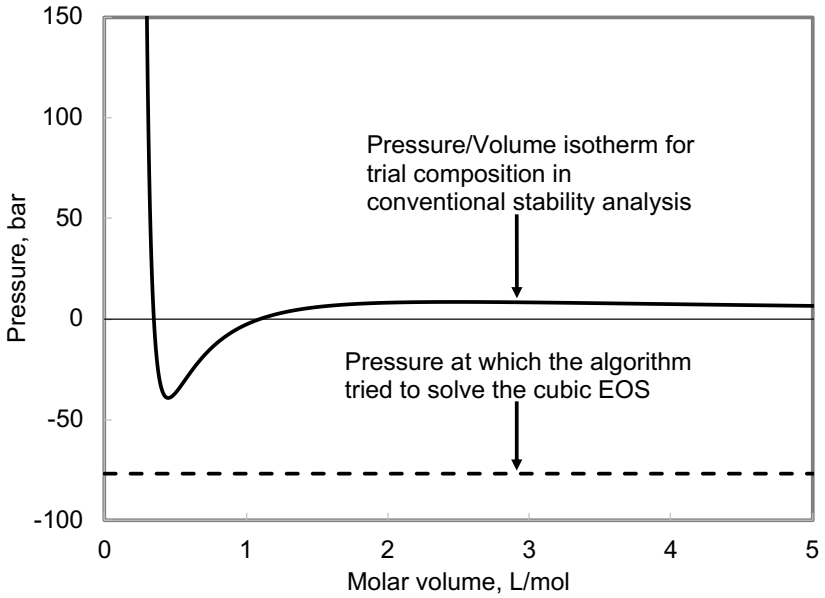

Figure 15: PV isotherm of liquid phase during iteration of Gibbs free energy-based algorithm. The lack of a physical solution to the EOS causes a non-convergence.

The new method has no such overshoot problems because it does not use iterative capillary pressure estimations as shown in Section 3.1.2. Also, it uses the minimization algorithm with the linear constraints, $\mathbf{b} \cdot \mathbf{d} < 1.0$. It is a standard procedure that keeps the iterate feasible in the algorithm, as used also by Nichita (2017).

3.2.3.2 Region II

In Region II, the conventional method results in non-convergence because of the absence of any solution to the phase-split calculation as part of phase stability analysis. In previous studies (Rezaveisi et al., 2018; Neshat et al., 2018), the fluid was assumed to be stable when their phase stability analysis methods resulted in this type of non-convergence. However, Figure 14 clearly shows that Region II exists even within the two-phase envelope. The robustness of the new method enables us to demonstrate for the first time that phase stability problems with capillary pressure can yield indefinite solutions.

A specific example is given using the same mixture (Table 5) at 644.3 K and the reference phase pressure of 81.3 bar. The new method converges rapidly to the solution with $D_{SP} = -1.80$ mol/L < 0 indicating the instability of the reference phase. Figure 18 shows the convergence behavior that is quadratic near the solution.

The conventional method using the Gibbs fee energy shows non-convergence as shown in Figure 17. The main reason for this non-convergence is that the iterative capillary pressure exceeds the capillary pressure at which the iterative liquid-like incipient phase is located at a spinodal point on the Gibbs free energy. With a capillary pressure greater than this limit, no solution exists for two-phase split calculation as explained in Shapiro and Stenby (2001).

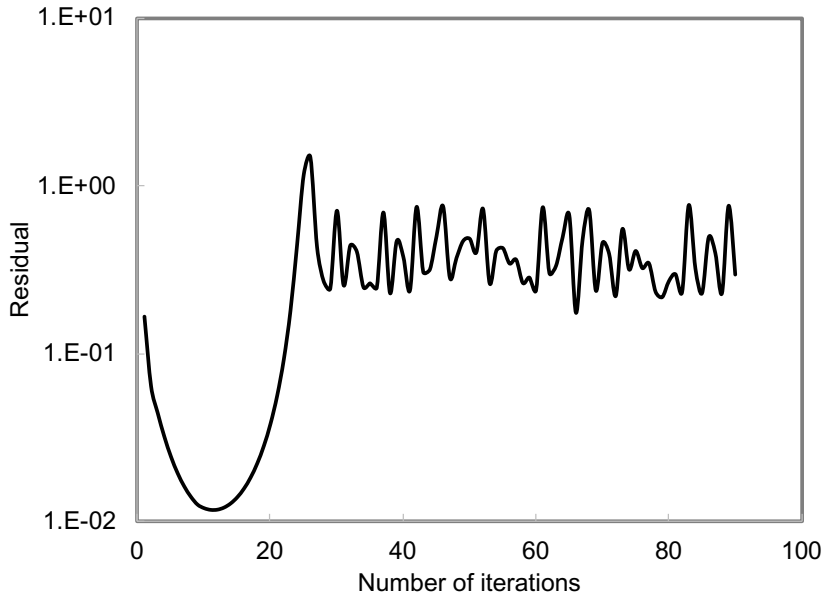

Figure 16: Non-convergence of phase-split calculation as a part of the stability analysis based on Gibbs free energy.

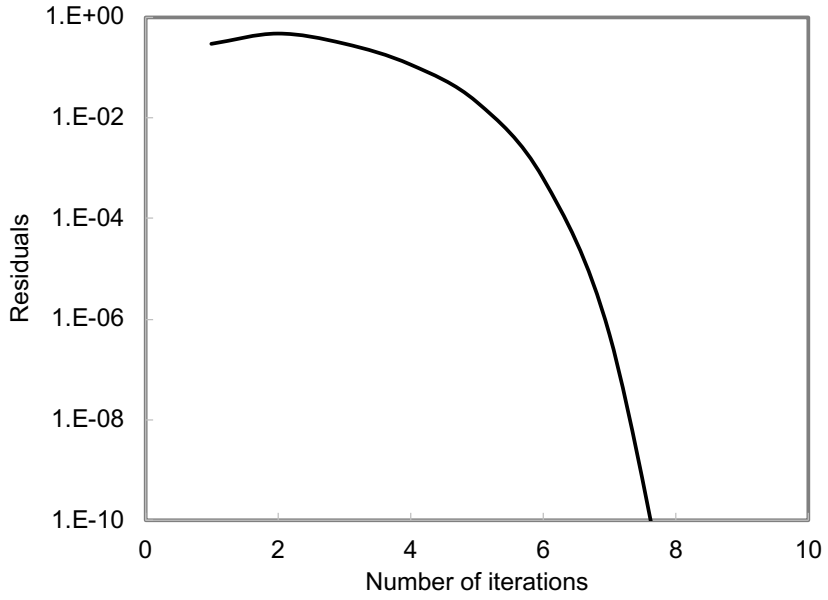

Figure 17: Quadratic convergence behavior of new stability analysis algorithm with an equimolar mixture of eagle ford light oil and methane in region II.

The new method clearly indicates that this type of indefinite situations occurs where the fluid is unstable ($D_{SP} < 0$), but has no solution of two equilibrium phases because of the capillary pressure model specified. It is important to recognize that the P_* term depends not only on the phase properties, but also on local details of the interface that cannot be described rigorously by a simple capillary pressure model.

3.2.4 Case 4

The traditional tangent-plane distance (TPD) function of Michelsen (1982a) gives a stationary point with a negative TPD value inside the two-phase region. In a single-phase region of pressure, temperature, and composition space, however, the TPD function exhibits either a stationary point with a positive TPD value or no stationary point except for the reference phase (i.e., the trivial solution). The thermodynamic conditions for such stationary points with positive TPD values are referred to as a "shadow-phase region" by Rasmussen et al. (2006). Such a shadow-phase region occurs between the two-phase region and the region of no non-trivial stationary point. Rasmussen et al. (2006) proposed a method to not perform phase stability analysis outside of the shadow phase region during equation-of-state compositional flow simulation for computational efficiency.

In the presence of capillary pressure, the shadow-phase region the Gibbs shadow phase region is irrelevant, and the Helmholtz shadow phase region is relevant, correct, and useful. The example used is based on the "SJ15" fluid as shown in Figure 19. The solid line shows the phase envelope boundary with no capillary pressure. The dashed line shows the outer boundary of the Gibbs shadow-phase region by Rasmussen et al. (2006) (i.e., no capillary pressure is considered). The bold dashed line shows the outer boundary of the Helmholtz shadow-phase region using the new method. Figure 19 shows that near the

bubble point, the Gibbs shadow-phase region is enclosed by the Helmholtz shadow-phase region. However, this observation is not general as confirmed in other cases.

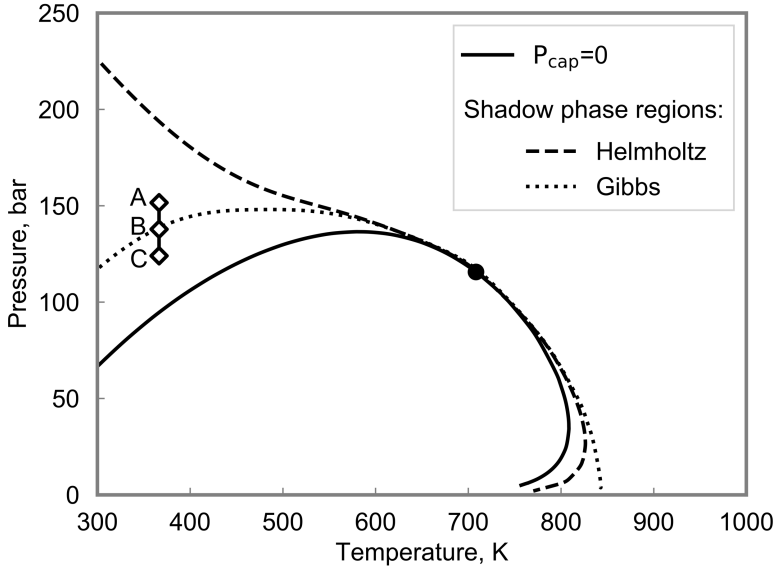

Figure 18: Helmholtz and Gibbs free energy shadow-phase regions with the for SJ15 oil mixture. Conditions A, B, and C indicate sample points where the phase behavior is analyzed in the presence of capillary pressure.

Here, we present an example to demonstrate the irrelevance of the Gibbs free energy shadow phase region. Figure 19 shows three selected points A, B, and C at 366.5 K, for each of which phase-split calculations are performed with different capillary pressures. Figure 20 shows the resulting gas phase mole fractions for points A, B, and C. Each of those points are inside the Helmholtz shadow-phase region and the SJ15 mixture has two phase solutions for certain ranges of capillary pressure. This is true even for point A which is outside the Gibbs free energy shadow-phase region of the SJ15 mixture. Point B is on the edge of the Gibbs shadow-phase region which seems to have no fundamental effect on phase behavior when considering capillary pressure. Finally, point C is inside both shadow-phase regions and also shows instability.

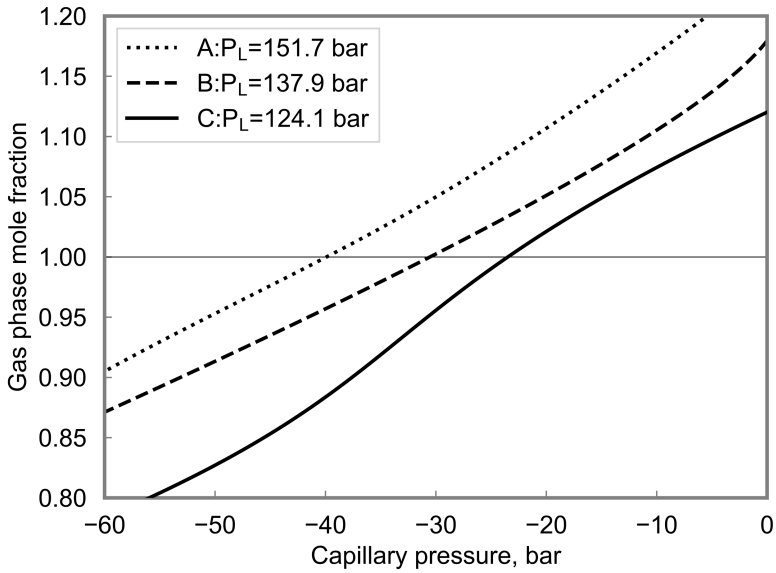

Figure 19: Oil phase mole fraction isobars with capillary pressure for liquid phase pressures of 151.7, 137.9, and 124.1 bar at points A, B, and C respectively as indicated on Figure 19. The temperature is 366.5 K.

Figure 21 shows another example analyzing the Gibbs and Helmholtz shadow-phase region using EF mixture (Tables 5 and 6). Figure 21 presents the two-phase boundary with a solid line, the outer boundary of the Gibbs shadow-phase region with a thin dashed line, and the outer boundary of the Helmholtz shadow-phase region with a bold dashed line. Figure 21b shows three selected points at 34.5 bar, for each of which phase-split calculations are performed with different capillary pressures. Figure 22 shows the resulting gas phase mole fractions for Points D, E, and F. The hollow circle for each curve corresponds to the capillary pressure beyond which no solution exists for the phase-split calculations (positive and negative flash). Point D is on the edge of the Gibbs shadow-phase region, but no capillary pressure value allows for a stable two-phase solution at this condition. Point E is on the edge of the Helmholtz shadow-phase region and has a stable two-phase solution only with the capillary pressure of 34.5 bar. Point F is located deep

inside the Helmholtz shadow-phase region in Figure 21b. There is a range of capillary pressures that make stable two-phase solutions as shown by the solid line in Figure 22. The D function shows a stationary point that is not the reference phase because it is inside the Helmholtz shadow-phase region.

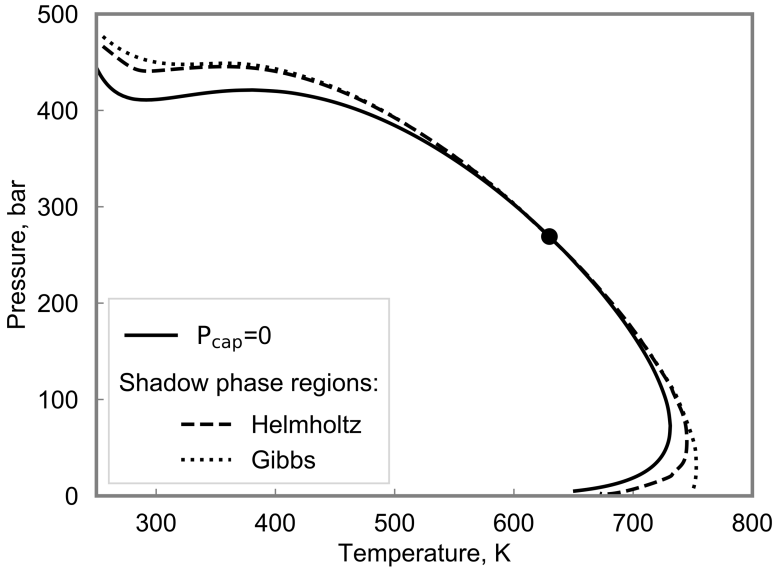

(a)

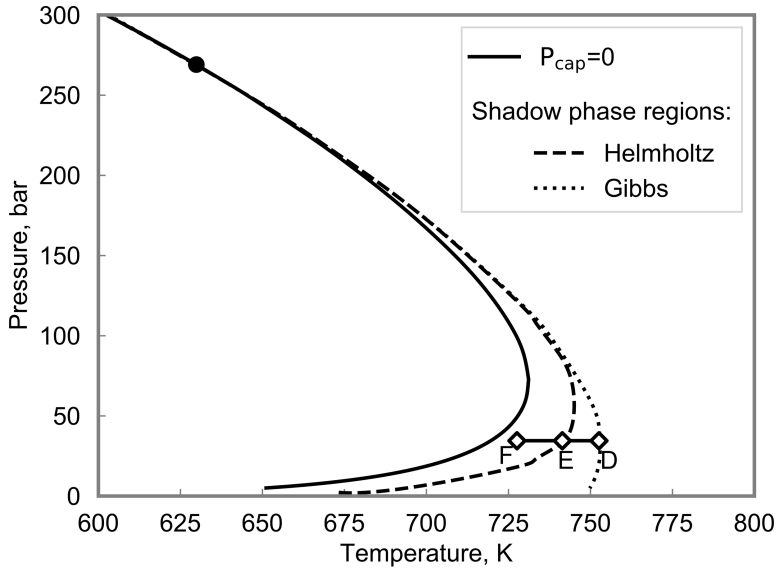

(b)

Figure 20: Helmholtz and Gibbs free energy shadow-phase regions for equimolar mixture of Eagle ford light oil and methane.

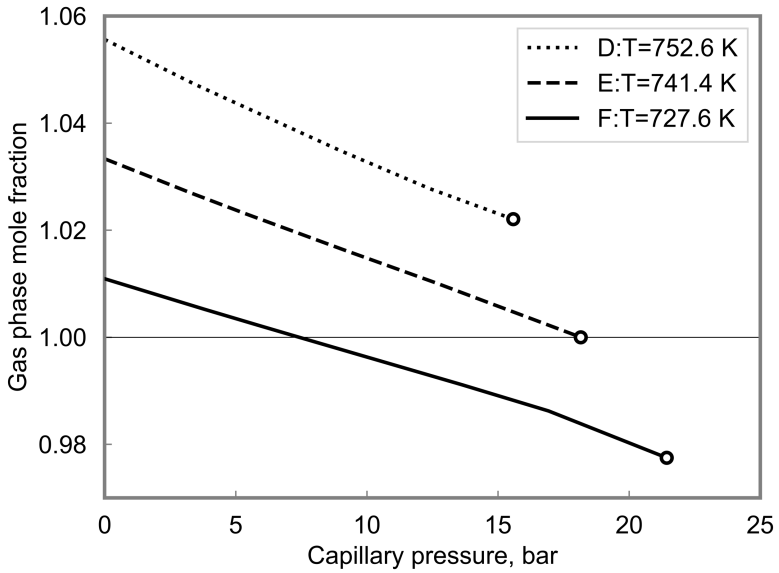

Figure 21: Oil phase mole fraction isotherms with capillary pressure for temperatures of 151.7, 137.9, and 124.1 bar at points A, B, and C respectively at 366.5 K as indicated in Figure 21b.

CHAPTER 4: Summary, Conclusions, and Future Research

4.1 SUMMARY AND CONCLUSION

In this report, we presented an algorithm using the Helmholtz free energy to investigate the stability of mixtures instead of the Gibbs free energy which is the conventional method for this calculation. The advantage of using the Helmholtz free energy is that the stability analysis can be completely decoupled from equilibrium capillary pressure calculations.

- The new algorithm is consistent with Gibbs free energy-based methods as opposed to previously published ones based on the Helmholtz free energy (Nichita, 2019a) because it recognizes that the P_* term can only be evaluated with capillary pressure models for incipient phases where the fugacity is equal to that of the reference phase.
- The new algorithm is robust at conditions where the conventional method systematically fails because:
    - It is not necessary to iteratively estimate the capillary pressure.
    - It does not need to run phase-split calculations in order to estimate the capillary pressure. Phase-split calculations as a part of conventional stability analysis diverge when the capillary pressure is large than that at the spinodal limit.
    - It takes advantage of a more predictable geometry with a single free energy surface instead of N_p non-linear surfaces of the Gibbs free energy.
- The shadow region in the presence of capillary pressure is correctly defined with the Helmholtz free energy but not with the Gibbs free energy.
- This report presented the first method of stability analysis for tight reservoirs modeled by a saturation-based capillary pressure that does not need to be coupled with a phase-split calculation.

- Our algorithm can be used with either Young-Laplace or saturation-based capillary pressure models. However, the saturation-based model gives better representation of rock physics.

4.2 FUTURE RESEARCH

The complexity of enhanced oil recovery for tight oil and gas reservoirs requires a general method to model multiphase equilibrium calculations including the effects of capillary pressure. This requires the development of robust phase-split calculations including the effects of capillary pressure and their implementation in a reservoir simulator. Several papers assumed that the mixture was stable when the phase-split calculation failed. This type of indefiniteness often occurs when conventional phase-split calculations are applied with capillary pressure.

A potential solution would be achieved by developing new methods to confirm the lack of solution for given conditions of the reference phase. The magnitude of the capillary pressure determines the smallest eigen-value of the Helmholtz Hessian and the existence of an equilibrium solution or lack thereof (Rezaveisi et al., 2018). Therefore, it is possible to numerically detect the lack of solution when necessary by using the free energy Hessian and the magnitude of the capillary pressure. Even though no method has been published to achieve this goal, it is of capital importance for the implementation of into reservoir simulators which compute a very large number of flash calculations.

The speed-up method of Rasmussen et al. (2006) for flash calculations in reservoir simulators can be implemented for tight reservoirs. The reported speed-up factor from the simplest reservoir simulation method is as high as 90% for non-tight reservoirs, although the speed-up factor depends on many other factors. This method heavily relied on the Gibbs shadow-phase region to determine whether or not to bypass the stability analysis. This work presented in this report showed that the Helmholtz shadow-phase region is the correct one to be used for tight reservoirs, therefore it has the potential to lead speeding up the compositional reservoir simulation for tight formations.

Several terms were neglected in the derivation of the Helmholtz TPD criterion. However, these terms can have a strong effect on the phase behavior of hydrocarbon mixtures in tight porous media with high surface-area-to-volume ratios. Multicomponent adsorption models can be coupled with phase equilibrium calculations (Sandoval et al, 2018). Additionally, canonical ensemble calculations and molecular dynamics simulations show that the intermolecular potentials of the pore walls also have a strong effect on phase behavior (Singh et al., 2009) in nanometer-sized pores. One approach to model this effect is by modifying the equations of state to account for the pore-wall potentials. Such was done by Barbosa et al. (2019) and many other authors. These models are usually validated by fitting experimentally measured adsorption isotherms. However, adsorption isotherms are usually measured only for pure substances or binary mixtures and tend to have very simple shapes which can be fit by many models without the necessity of them being physically correct or useful. Therefore, a new practical approach is necessary to rigorously model hydrocarbon mixture phase behavior in tight porous media, including multicomponent adsorption.

Appendices

APPENDIX A: STABILITY ANALYSIS ALGORITHM USING GIBBS FREE ENERGY

This section presents the general algorithm for coupled phase-stability and phase-split calculation algorithm including the effect of capillary pressure. The conventional root selection method is not robust; therefore, the roots are selected based on user-input. For all of the cases tested in chapter 3, selecting the upper root for the gaseous phase and the lower root for the liquid phase converged to the correct solution. The stability analysis uses the composition **y,** and the phase-split calculation uses composition **x**. The detailed algorithm is then written as follows.

Step 1. Minimize the TPD at 0 capillary pressure.

1.1 Compute the compressibility factors of the reference phase at the reference phase pressure P_r by solving the cubic EOS (2.45). Select the root based on the lowest Gibbs free energy criterion.

1.2 Compute the initial guesses for the trial phase independent variables using Wilson's correlation.

1.3 Compute the composition of the trial phase $y_i = X_i / \sum_{i=1}^{N_c} X_i$.

1.4 Compute the compressibility factors and fugacity coefficients for the trial phase at $P_t = P_r$. If necessary, select the correct root based on the lowest Gibbs free energy criterion.

1.5 If the maximum norm of the set of stationarity equations (2.31) is less than a specified tolerance ε_{GS}, go to step 1.7. Otherwise, go to step 1.8.

1.6 Update the independent variables **X** using equation (2.68) and return to step 1.4.

1.7 Identify the unique non-trivial stationary points found. If both initial guesses converge to the trivial solution, stop. This mixture forms a stable single

phase. Otherwise, set the composition with highest value of $\sum_{i=1}^{N_c} X_i$ to $\mathbf{y}$ and go to Step 2.

Step 2. Determine whether the reference phase $\mathbf{z}$ is liquid or vapor based on properties of compositions $\mathbf{z}$ and $\mathbf{y}$. Compute the K-values initial guess based on the reference and trial phase compositions such that $K_i = x_{iV}/x_{iL}$ $(i = 1, \dots, N_c)$. Set $P_L = P_V = P_r$.

Step 3. Run a phase split calculation at constant capillary pressure.

3.1 Calculate the phase mole fractions and phase compositions using a constant K-flash calculation.

3.2 Solve the cubic EOS for compressibility factor and compute the fugacity for both phases.

3.3 If the maximum norm of the fugacity equations vector is less than a specified tolerance ε_{PS}, go to step 4. Otherwise go to step 3.4

3.4 Use equation (2.67) to update the K-values and return to step 3.1.

Step 4. Compute the capillary pressure for the converged liquid and vapor phases from the phase-split calculation. If the reference phase is vapor, set $P_V = P_r$ and $P_t = P_L = P_r - P_{cap}$. Otherwise, set $P_L = P_r$ and $P_V = P_t = P_r + P_{cap}$.

Step 5. Evaluate the residual based on the change of capillary pressure $r = \left|(P_{cap}^{old} - P_{cap}^{new})/P_{cap}^{new}\right|$. If r is less than a specified convergence criterion ε_{OL}, stop. Otherwise, continue to step 6.

Step 6. Minimize the TPD at the trial phase pressure P_t using initial guess $\mathbf{X} = \mathbf{y}$.

6.1 Compute the compressibility factors of the reference phase by solving the cubic EOS (2.45). Select the root based on user-input.

6.2 Compute the composition of the trial phase $y_i = X_i / \sum_{i=1}^{N_c} X_i$.

6.3 Compute the compressibility factors and fugacity coefficients for the trial phase. If necessary, select the correct root based on user-input.

6.4 If the maximum norm of stationarity equations (2.31) is less than a specified tolerance ε_{GS}, go to step 3. Otherwise, go to 1.7.

6.5 Update the independent variables **X** using equation (2.68) and return to step 1.4.

The phase identification is done with respect to the co-volume parameters of the reference phase and that of the stationary point as described in Chapter 3.

The root-selection method must also be able to detect cases where non-physical solutions exist such as demonstrated in Figure 16. This general method for determining all the physical roots available is the following.

Step 1. Solve the cubic EOS for the compressibility factor.

Step 2. Set the number of real roots to the EOS to N.

Step 3. Compute the molar volume $\underline{V}_i$ $(i = 1, \dots, N)$.

Step 4. If $N = 1$, and $\underline{V}_1 < b_m$, then the pressure is non-physical, stop. If $N = 1$, and $\underline{V}_1 > b_m$, the pressure is physical, return $\underline{V}_1$ and Z_1 as the solution to the EOS. Otherwise, go to step 5.

Step 5. If $\underline{V}_3 < b_m$, then the pressure is non-physical, stop. Otherwise, the pressure is physical and $\underline{V}_3$ is a valid root of the EOS. Continue to step 6.

Step 6. If $\underline{V}_2 < b_m$, then there is only one physical root of the EOS $\underline{V}_3$. Otherwise, $\underline{V}_2$ is a physical root of the EOS. Continue to step 7.

Step 7. If $\underline{V}_2 < b_m$, then there are only two physical roots of the EOS, $\underline{V}_3$ and $\underline{V}_2$. Otherwise, the pressure is physical and $\underline{V}_1$ is a physical root of the EOS and the middle root $\underline{V}_2$ is intrinsically unstable.

APPENDIX B: HELMHOLTZ FREE ENERGY TPD HESSIAN AND GRADIENT

This section presents the equation for the Hessian of the Helmholtz free energy in terms of the independent variable $\boldsymbol{\delta}$. For simplification purposes, we introduce the following intermediary variables

$$\kappa = \frac{\underline{V}}{b_m};\ \beta_i = \frac{b_i}{b_m};\ \theta_i = \frac{\sum_{j=1}^{N_c} x_j \sqrt{a_i a_j}\left(1 - k_{ij}\right)}{a_m};\ \zeta_1 = \frac{1}{\kappa - 1};$$

$$\zeta_2 = 2\left(\frac{\left(1+\sqrt{2}\right)}{\kappa + \left(1+\sqrt{2}\right)} - \frac{\left(1-\sqrt{2}\right)}{\kappa + \left(1-\sqrt{2}\right)}\right)/2\sqrt{2}$$

$$\zeta_3 = \left(\left(\frac{\left(1+\sqrt{2}\right)}{\kappa + \left(1+\sqrt{2}\right)}\right)^2 - \left(\frac{\left(1-\sqrt{2}\right)}{\kappa + \left(1-\sqrt{2}\right)}\right)^2\right)/2\sqrt{2}$$

$$\zeta_5 = 2\ln\left[\frac{\kappa + \left(1+\sqrt{2}\right)}{\kappa + \left(1-\sqrt{2}\right)}\right]/2\sqrt{2};\ \zeta_6 = \zeta_2 - F_5$$

The Napierian logarithm of the fugacity can then be derived as a function of the pseudo-variables defined above as

$$\ln(f_i) = \beta_i\zeta_1 + \ln(x_i\zeta_1 RT/b_m) - a_m/RTb_m(\theta_i\zeta_5 + \beta_i\zeta_6/2), \text{ where } i = 1, \ldots, N_c$$

The gradient of the Helmholtz free energy TPD is then

$$\boldsymbol{\nabla} D_i = (\partial D/\partial \alpha_i)_{T,\alpha_{j\neq i}} = (\ln(f_i) - \ln(f_{ir}))\delta_i/2.$$

Finally, the expression for the Helmholtz free energy TPD Hessian is

$$H_{ij} = \left(\partial^2 D/\partial\delta_i\partial\delta_j\right)_{T,\delta_{k\neq i,j}} = \left(\partial(\ln(f_i)\,\delta_i/2)/\partial\delta_j\right)_{T,\delta_{k\neq i,j}}$$

$$H_{ij} = \left(\left(\beta_i + \beta_j + \beta_i\beta_j\zeta_1\right)\zeta_1 + (RTb_m)^{-1}\left(a_m\left(\beta_i\beta_j(\zeta_3 + \zeta_6) - \zeta_6\left(\beta_i\theta_j + \beta_j\theta_i\right)\right) - \zeta_5 a_{ij}\right)\right)\sqrt{x_i x_j} + \delta_{ij}, \text{ where } i = 1, \ldots, N_c \text{ and } j = 1, \ldots, N_c$$

Glossary

Roman symbols

a	Attraction parameter for the Peng-Robinson equation of state
a_o	Saturation-based capillary pressure parameter defined in section 2.1.4.3
a_g	Saturation-based capillary pressure parameter defined in section 2.1.4.3
$\mathrm{a_{ij}}$	Interfacial area separating phases i and j
$\mathbf{a}$	Vector defining the lower bound for a general linear constraint
A	Helmholtz free energy
b_o	Saturation-based capillary pressure parameter defined in section 2.1.4.3
b_g	Saturation-based capillary pressure parameter defined in section 2.1.4.3
b	Co-volume parameter for the Peng-Robinson equation of state
$\mathbf{C}$	General matrix for local minimization equation defined in section 2.1.5
d	Differential change operator
$\boldsymbol{d}$	Vector representing a search direction
$\underline{\mathbf{d}}$	Vector representing the component molar densities of a mixture
$\mathrm{d_i}$	Component i molar density
D	Tangent plane distance to a thermodynamic function
E	Energy carried by the flow of matter
$\mathrm{f_{ij}}$	Fugacity of component i in phase j
$\boldsymbol{\mathcal{F}}$	Vector containing set of equations to be solved
F	General objective function to be minimized
$\mathrm{F_i}$	ith stationarity condition for the Helmholtz free energy TPD
$\mathbf{f}$	Vector containing Rachford-Rice equations
$\mathbf{g}$	Gradient of the Helmholtz free energy TPD
$\boldsymbol{\mathcal{G}}$	General fixed-point iteration function
G	Gibbs free energy
$\underline{\mathrm{G}}_\mathrm{R}$	Dimensionless molar Gibbs free energy
h	Length of capillary tube wetted by the vapor phase
$\mathbf{H}$	Hessian matrix
J	Jacobian matrix
k	Permeability of a porous medium
$\mathrm{k_{ij}}$	Binary interaction parameter for component i and j
$\mathrm{K_{ij}}$	K-value of component i in phase j
l	Total length of capillary tube
$\mathcal{M}$	General thermodynamic variable
$\overline{\mathcal{M}_\mathrm{i}}$	General form of a partial molar property for component i
$\mathrm{n_{ij}}$	Number of moles of component i in phase j
$\underline{\mathbf{n}}$	Vector containing the mole numbers for each component in each phase
$\mathrm{N_c}$	Number of components
$\mathrm{N_f}$	Number of interfaces

N_p Number of phases
N_t Number of subsystems
P Pressure
P_* Term derived for new stability test
P_{cap} Capillary pressure
P_i^{vap} Vapor pressure for component i
Q Heat
R Ideal gas constant
$\mathcal{R}$ Capillary tube radius
S Entropy
t_i Intermediary variable used in K-flash for component i
T Temperature or equation for the tangent plane to a surface
T_{ci} Critical temperature for component i.
U Internal energy
$\mathbf{U}$ Variable transformation matrix
V Volume
$\underline{V}$ Molar volume
$\overline{\underline{V}}_i$ Partial molar volume of component i
W Work
x_{ij} Mole fraction of component i in phase j
$\mathbf{x}$ Vector containing component phase mole fraction
y_i Mole fraction of component i used for stability analysis
Y Generalized force term in the expression for work
X_i Independent variable for component i used for stability analysis
X Generalized displacement term in the expression for work
z_i Mole fraction of component i in the reference phase
Z_i Compressibility factor for the ith root of the cubic equation of state

Greek letters

α Parameter for Peng-Robinson EOS defined in section 2.1.3
β_j Mole fraction of phase j
β_i Dimensionless intermediary variable for component i defined in Appendix B
γ Parachor exponent
γ Phase-dependent parameter in the TPD derived by Kou and Sun (2018)
Δ Finite difference
δ_{ij} Independent variable defined in section 2.2.2
$\boldsymbol{\delta}$ Vector of independent variables independent variable defined in section 2.2.2
δ_{ij} Kronecker delta
ε Tolerance for convergence criterion
ζ_j Dimensionless intermediary variable defined in Appendix B
θ Contact angle
θ_i Dimensionless intermediary variable for component i defined in Appendix B

κ	Parameter for Peng-Robinson EOS defined in section 2.1.3
κ	Dimensionless volume defined in Appendix B
λ	Step-size for minimization algorithm
μ_{ij}	Chemical potential for component i in phase j
Π_i	Parachor coefficient for component i
ρ_j	Mass density for phase j
σ	Interfacial tension or other interfacial property when used as a subscript
ϕ_{ij}	Fugacity coefficient of component i in phase j
ϕ	Porosity
ω	Acentric factor
ϖ	Angle between two vectors
$\boldsymbol{\nabla}$	Vector differential operator

Superscripts

bbl	Bubble point
dew	Dew point
IGM	Ideal gas mixture
k	Index for iteration steps
$'$	Thermodynamic property of the surroundings

Subscripts

g	Gas
n	Component mole number variable space
lnK	K-value logarithm variable space
L	Liquid
m	Mixture
min	Minimum
o	Oil
r	Reference
R	Reduced
s	Boundary or solid surface
SP	Stationary point
t	Trial phase
total	Total mixture property
T	System where interfacial energy is negligible
V	Vapor

Abbreviation

BIP	Binary interaction parameters
EOS	Equation of state
IFT	Interfacial tension
PR	Peng-Robinson
TPD	Tangent plane distance

References

Al-Doury, M.M.I. (2010). A discussion about hydraulic permeability and permeability. *Petroleum Science and Technology*, *28*(17), 1740-1749.

Baker, L. E., Pierce, A. C., & Luks, K. D. (1982). Gibbs energy analysis of phase equilibria. *Society of Petroleum Engineers Journal*, 22(05), 731-742.

Castier, M. (2014). Helmholtz function-based global phase stability test and its link to the isothermal–isochoric flash problem. *Fluid Phase Equilibria*, 379, 104-111.

Dennis Jr, J. E., & Schnabel, R. B. (1996). *Numerical methods for unconstrained optimization and nonlinear equations*. SIAM, Philadelphia, PA.

Jindrová, T., & Mikyška, J. (2013). Fast and robust algorithm for calculation of two-phase equilibria at given volume, temperature, and moles. *Fluid Phase Equilibria*, 353, 101-114.

Jindrová, T., & Mikyška, J. (2015). General algorithm for multiphase equilibria calculation at given volume, temperature, and moles. *Fluid Phase Equilibria*, 393, 7-25.

Kou, J., & Sun, S. (2018). A stable algorithm for calculating phase equilibria with capillarity at specified moles, volume and temperature using a dynamic model. *Fluid Phase Equilibria*, 456, 7-24.

Gibbs, J. W. (1878). On the equilibrium of heterogeneous substances. *American Journal of Science*, (96), 441-458.

Gill, P. E., & Murray, W. (1974). Newton-type methods for unconstrained and linearly constrained optimization. *Mathematical Programming*, 7(1), 311-350.

Kumar, A., & Okuno, R. (2015). Direct perturbation of the Peng–Robinson attraction and covolume parameters for reservoir fluid characterization. *Chemical Engineering Science*, 127, 293-309.

Lee, S. T., & Chien, M. C. H. (1984, January). A new multicomponent surface tension correlation based on scaling theory. In SPE Enhanced Oil Recovery Symposium. Society of Petroleum Engineers.

Leibovici, C. F., & Neoschil, J. (1995). A solution of Rachford-Rice equations for multiphase systems. *Fluid Phase Equilibria*, 112(2), 217-221.

Li, Z., & Firoozabadi, A. (2012). General strategy for stability testing and phase-split calculation in two and three phases. *SPE Journal*, 17(04), 1-096.

Mehra, R. K., Heidemann, R. A., & Aziz, K. (1983). An accelerated successive substitution algorithm. *The Canadian Journal of Chemical Engineering*, 61(4), 590-596.

Michelsen, M. L. (1982a). The isothermal flash problem. Part I. Stability. *Fluid phase equilibria*, 9(1), 1-19.

Michelsen, M. L. (1982b). The isothermal flash problem. Part II. Phase-split calculation. *Fluid phase equilibria*, 9(1), 21-40.

Michelsen, M. L., & Heidemann, R. A. (1988). Calculation of critical points from cubic two-constant equations of state. *AIChE journal*, 27(3), 521-523.

Michelsen, M. L. (1994). Calculation of multiphase equilibrium. *Computers & chemical engineering*, 18(7), 545-550.

Mikyška, J., & Firoozabadi, A. (2012). Investigation of mixture stability at given volume, temperature, and number of moles. *Fluid Phase Equilibria*, 321, 1-9.

Nagarajan, N. R., Cullick, A. S., & Griewank, A. (1991). New strategy for phase equilibrium and critical point calculations by thermodynamic energy analysis. Part I. Stability analysis and flash. *Fluid Phase Equilibria*, 62(3), 191-210.

Neshat, S. S., Okuno, R., & Pope, G. A. (2018). A rigorous solution to the problem of phase behavior in unconventional formations with high capillary pressure. *SPE Journal*, 23(04), 1-438.

Neshat, S. S., Okuno, R., & Pope, G. A. (2019, March). Thermodaynamic Stability Analysis for Multi-Component Mixtures with Capillary Pressure. In SPE Reservoir Simulation Conference. Society of Petroleum Engineers.

Nichita, D. V., Valencia, C. D. L. A. D., & Gomez, S. (2006). Volume-based thermodynamics global phase stability analysis. *Chemical Engineering Communications*, 193(10), 1194-1216.

Nichita, D. V., De-Hemptinne, J. C., & Gomez, S. (2009). Isochoric phase stability testing for hydrocarbon mixtures. *Petroleum Science and Technology*, 27(18), 2177-2191.

Nichita, D. V. (2017). Fast and robust phase stability testing at isothermal-isochoric conditions. *Fluid Phase Equilibria*, 447, 107-124.

Nichita, D. V. (2018). Volume-based phase stability testing at pressure and temperature specifications. *Fluid Phase Equilibria*, 458, 123-141.

Nichita, D. V. (2019a). Volume-based phase stability analysis including capillary pressure. *Fluid Phase Equilibria*, 492, 145-160.

Nichita, D. V. (2019b). Density-based phase envelope construction including capillary pressure. *Fluid Phase Equilibria*, 498, 33-44.

Okuno, R. (2009). *Modeling of multiphase behavior for gas flooding simulation.* PhD dissertation, the University of Texas at Austin, Austin, Texas.

Okuno, R., Johns, R., & Sepehrnoori, K. (2010). A new algorithm for Rachford-Rice for multiphase compositional simulation. *SPE Journal*, 15(02), 313-325.

Orangi, A., Nagarajan, N. R., Honarpour, M. M., & Rosenzweig, J. J. (2011, January). Unconventional shale oil and gas-condensate reservoir production, impact of rock, fluid, and hydraulic fractures. In SPE hydraulic fracturing technology conference. Society of Petroleum Engineers.

Peng, D. Y., & Robinson, D. B. (1976). A new two-constant equation of state. *Industrial & Engineering Chemistry Fundamentals*, 15(1), 59-64.

Rachford Jr, H. H., & Rice, J. D. (1952). Procedure for use of electronic digital computers in calculating flash vaporization hydrocarbon equilibrium. *Journal of Petroleum Technology*, 4(10), 19-3.

Rasmussen, C. P., Krejbjerg, K., Michelsen, M. L., & Bjurstrøm, K. E. (2006, February 1). Increasing the Computational Speed of Flash Calculations With Applications for Compositional, Transient Simulations. *SPE Reservoir Evaluation & Engineering*. doi:10.2118/84181-PA.

Rezaveisi, M., Sepehrnoori, K., Pope, G. A., & Johns, R. T. (2018). Thermodynamic analysis of phase behavior at high capillary pressure. *SPE Journal*. 23(06), 1-14.

Robinson, D. B., & Peng, D. Y. (1978). The characterization of the heptanes and heavier fractions for the GPA Peng-Robinson programs. Gas processors association.

Schechter, D. S., & Guo, B. (1998). Parachors based on modern physics and their uses in IFT prediction of reservoir fluids. *SPE Reservoir Evaluation & Engineering*, 1(03), 207-217.

Shapiro, A. A., & Stenby, E. H. (2001). Thermodynamics of the multicomponent vapor–liquid equilibrium under capillary pressure difference. *Fluid Phase Equilibria*, 178(1-2), 17-32.

Sherafati, M., & Jessen, K. (2017). Stability analysis for multicomponent mixtures including capillary pressure. *Fluid Phase Equilibria*, 433, 56-66.

Siripatrachai, N., Ertekin, T., & Johns, R. T. (2017). Compositional simulation of hydraulically fractured tight formation considering the effect of capillary pressure on phase behavior. *SPE Journal*, 22(04), 1-046.

Soave, G. (1972). Equilibrium constants from a modified Redlich-Kwong equation of state. *Chemical engineering science*, 27(6), 1197-1203.

van der Waals, J.D. 1873. *On the Continuity of the Gaseous and Liquid States*. Edited and With an Introduction by Rowlinson, J.S. (1988) Dover Publications, Inc., New York.

Weinaug, C. F., & Katz, D. L. (1943). Surface tensions of methane-propane mixtures. *Industrial & Engineering Chemistry*, 35(2), 239-246.

Wilson, G. M. (1969, May). A modified Redlich-Kwong equation of state, application to general physical data calculations. In 65th National AIChE Meeting, Cleveland, OH (p. 15).

Yan, B., Wang, Y., & Killough, J. E. (2017). A fully compositional model considering the effect of nanopores in tight oil reservoirs. *Journal of Petroleum Science and Engineering*, 152, 675-682.